Genistein-Derived ROS-Responsive Nanoparticles Relieve Colitis by Regulating Mucosal Homeostasis

Wentao Fan, Shuo Zhang, Yuting Wu, Tao Lu, Jiwen Liu, Xiuyun Cao, Shuhui Liu, Liping Yan, Xizhi Shi, Guangliang Liu, Chaobo Huang, and Suquan Song*

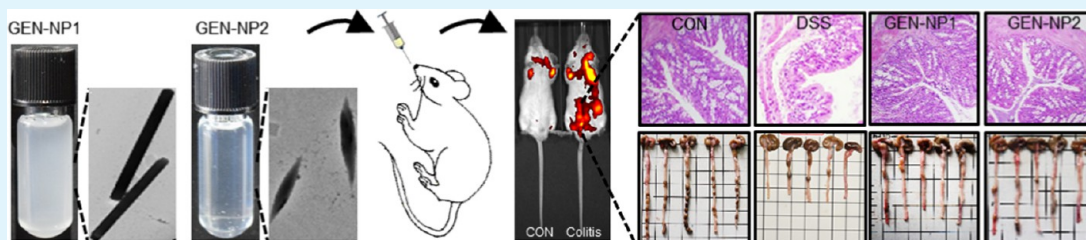Cite This: https://doi.org/10.1021/acsami.1c09215

Read Online

ACCESS | Metrics & More | Article Recommendations | Supporting Information

ABSTRACT: Disruption of intestinal homeostasis is an important event in the development of inflammatory bowel disease (IBD), and genistein (GEN) is a candidate medicine to prevent IBD. However, the clinical application of GEN is restricted owing to its low oral bioavailability. Herein, a reactive oxygen species (ROS)-responsive nanomaterial (defined as GEN-NP2) containing superoxidase dismutase-mimetic temporally conjugated β-cyclodextrin and 4-(hydroxymethyl)phenylboronic acid pinacol ester-modified GEN was prepared. GEN-NP2 effectively delivered GEN to the inflammation site and protected GEN from rapid metabolism and elimination in the gastrointestinal tract. In response to high ROS levels, GEN was site-specifically released and accumulated at inflammatory sites. Mechanistically, GEN-NP2 effectively increased the expression of estrogen receptor β (ERβ), simultaneously reduced the expression of proinflammatory mediators (apoptosis-associated speck-like protein containing a CARD (ASC) and Caspase1-p20), attenuated the infiltration of inflammatory cells, promoted autophagy of intestinal epithelial cells, inhibited the secretion of interleukin-1β (IL-1β) and tumor necrosis factor-α (TNF-α), modulated the gut microbiota, and ultimately alleviated colitis. In addition, the oral administration of these nanoparticles showed excellent safety, thereby providing confidence in the further development of precise treatments for IBD.

KEYWORDS: colitis, mucosal homeostasis, ROS-responsive, nanoparticles, genistein

INTRODUCTION

Inflammatory bowel disease (IBD), characterized as a kind of chronic intestinal disorder, is typically categorized into one of the two subtypes: Crohn's disease (CD) and ulcerative colitis (UC), which affect 6.8 million people worldwide.[1] Joint efforts in health-care innovation and disease prevention and treatment are required to alleviate the burden of IBD.[2] Accumulating evidence has revealed that the initiation and pathogenesis of IBD are highly related to mucosal homeostasis.[3,4] Therefore, the intestinal epithelium has attracted attention due to its function in nutrient absorption, its activity as a physical barrier, and its response to signals from the immune system and intestinal microbiota.[5] It has been well established that the mucosal immune system is the main mediator of IBD by driving the dysregulated immune response against commensal microflora.[6] On the other hand, although the epithelial layer provides a protective barrier, the gastrointestinal tract is the main source of reactive oxygen species (ROS). Pathogens and ingested materials can cause the production of inflammatory cytokines and other mediators, which further lead to oxidative stress.[7]

Excessive ROS production and continuous oxidative stress can induce local tissue injury and subsequent inflammation.[8,9] Immunosuppressants, aminosalicylates, and steroids are the main drugs used to treat IBD. However, these anti-inflammatory medications give rise to many side effects, such as vomiting, diarrhea, lymphopenia, allergic responses, inflammation of the pancreas, and increased liver enzymes.[10] More importantly, a large number of IBD patients are often unresponsive to conventional anti-inflammatory drugs.[10] Therefore, safer and more effective strategies must be developed to manage a variety of conditions related to IBD, including immune factor secretion, microbe behavior, dysregulation of the epithelium, and ROS accumulation.
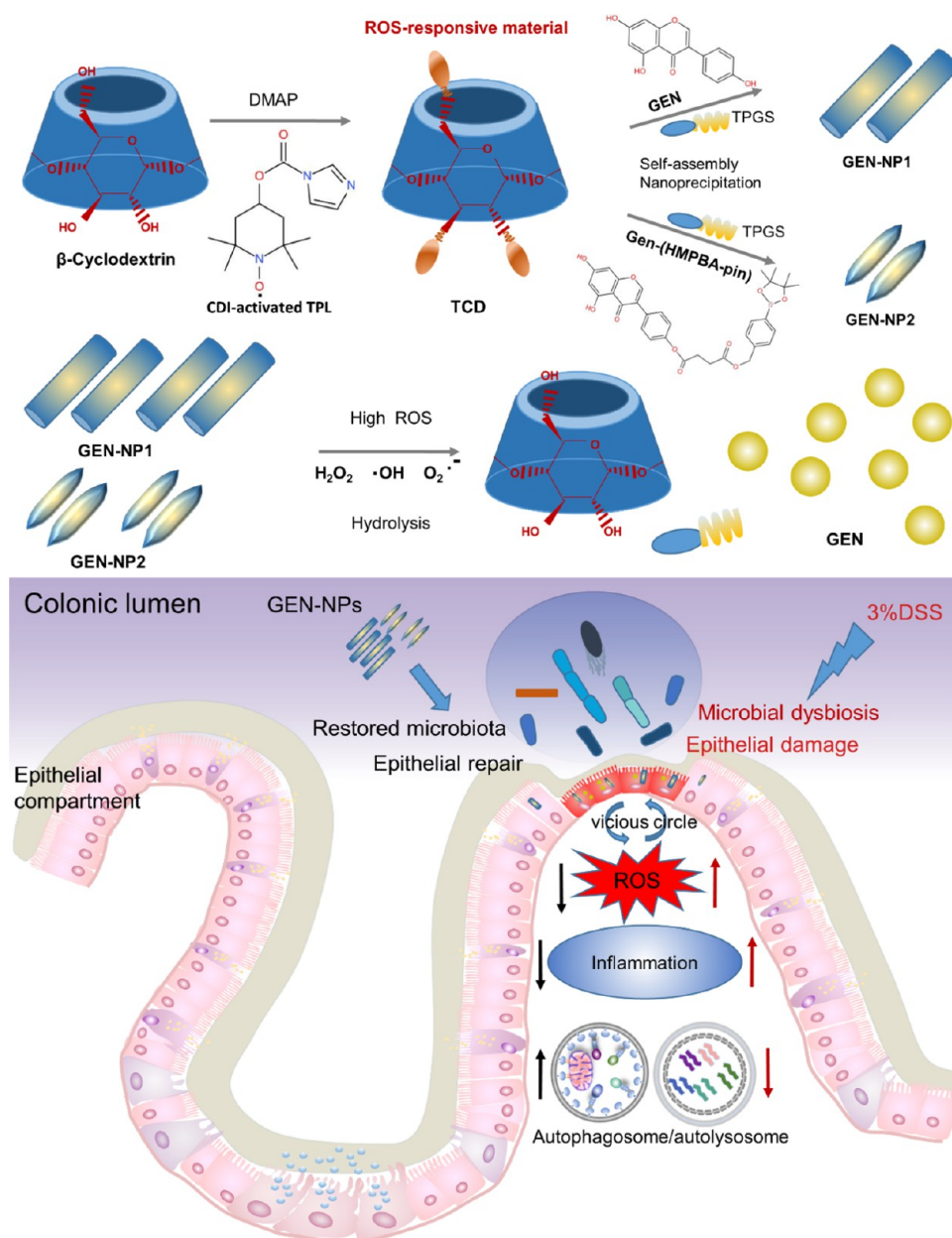
Figure 1. Schematic diagram of the genistein nanoparticle synthesis (GEN-NPs) and targeted treatment of colitis. β-cyclodextrin, β-CD; CDI, 1,1-carbonyldiimidazole; TPL, Tempol; DMAP, 4-dimethylaminopyridine; TCD, TPL-conjugated β-CD; GEN, genistein; TPGS, D-α-tocopherol poly(ethylene glycol) 1000 succinate; NPs, nanoparticles; and ROS, reactive oxygen species.

Numerous studies have confirmed that natural macro-molecules and phytochemicals can reduce IBD-related complications by modifying enzymatic activity, alleviating oxidative stress, inhibiting proinflammatory cytokine secretion, and regulating gut microbiota.[11,12] Therefore, these molecules derived from natural sources may present a safe, effective, and affordable approach to restraining the increasing burden of IBD throughout the world. It has been widely accepted that genistein (GEN), a biologically active isoflavone mainly exists in soy-based food, can regulate cellular and humoral immunity and suppress the secretion of granule enzymes to maintain homeostasis of inflammation.[13] Furthermore, GEN is a potent antioxidant agent that scavenges ROS and blocks oxidative stress[14] and may exert beneficial effects against colitis.[15−18] However, the low water solubility, poor oral bioavailability, and rapid metabolism of this compound severely hinder its

application.[19] Therefore, it is urgent to design a feasible and economical delivery system to enhance the bioavailability of GEN while maintaining its chemical stability and controlling its release at diseased sites.

Owing to their distinct advantages, such as high bioavail-ability, biocompatibility, targeting efficiency, and minimal toxicity, many nanoparticles (NPs) have been developed as effective drug delivery systems.[20,21] For example, anticancer nanomedicines can sequentially respond to the release of different cargos.[22] In particular, NPs can overcome the common barriers imposed by the intestine, which make them ideal for anti-colitis treatment.[11,23] Generally, an ideal drug delivery system for colitis treatment would be able to deliver drugs to the inflamed colon directly and reduce their side effects caused by systemic absorption. Meanwhile, the delivery system would allow escape from the biological defense system and extend the
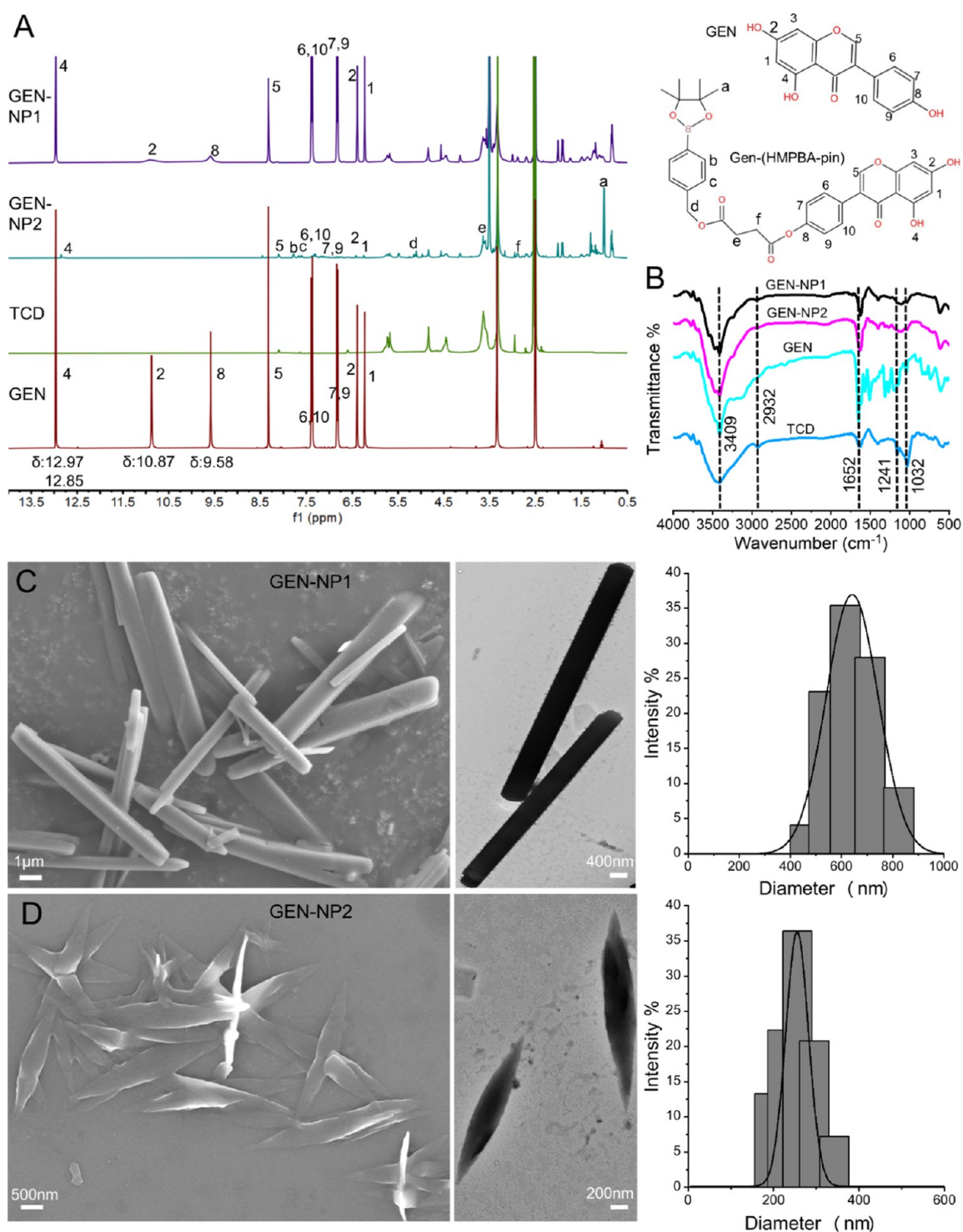
Figure 2. Characterization of GEN-NPs. (A) ^{1}H nuclear magnetic resonance spectroscopy of different materials, namely, GEN-NP1, GEN-NP2, TCD, and GEN. (B) Fourier transform infrared spectra of GEN-NP1, GEN-NP2, TCD, and GEN. (C, D) Scanning electron microscopy images (left), transmission electron microscopy micrographs (middle), and size distribution profiles (right) of GEN-NP1 and GEN-NP2. Scale bars represent the values indicated.

retention time of the drug at the target.[24] Moreover, the NP surface can be modified according to different endogenous (enzyme, pH, and redox) or exogenous (ultrasound, magnetic, and light) stimuli.[25] Since colitis is accompanied by excessive ROS production, the development of an ROS-responsive drug delivery system for IBD treatment shows broad prospects.[26,27] Although some GEN-NPs have been synthesized previ-

ously,[19,28,29] ROS-triggered drug delivery systems, which can release GEN at the inflamed site, have not been investigated. Therefore, in this research, a novel ROS-responsive nanomaterial for site-specific delivery of GEN was developed, and the treatment effects and mechanism of this nanotherapy were systematically studied (Figure 1).
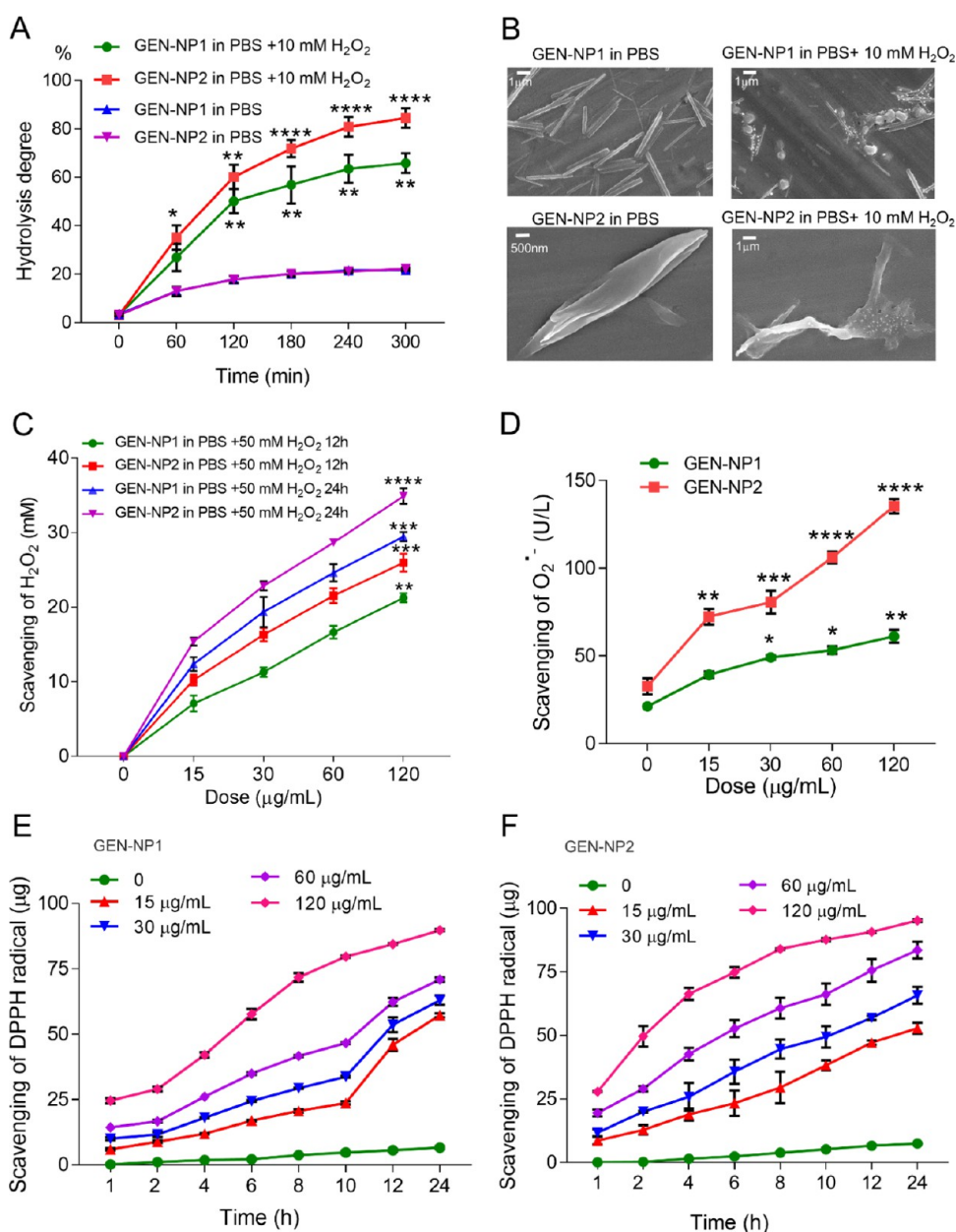
Figure 3. ROS-scavenging capability of GEN-NPs. (A) Hydrolysis curves of GEN-NPs in PBS (0.01 M, pH 7.4) with 10 mM H_2O_2. (B) Scanning electron microscopy of GEN-NPs after hydrolysis in 10 mM H_2O_2. (C) H_2O_2-scavenging efficiency of GEN-NPs at different doses and incubation times. (D) Removal of $O_2^{\bullet-}$ by GEN-NPs after incubation for 50 min. (E, F) Dose- and time-dependent elimination of DPPH radicals. Data are shown as the mean ± S.E.M. ($n = 3$). Statistical significance was evaluated via two-way ANOVA with Dunnett's post hoc test for the data in (A−D). *$P < 0.05$, **$P < 0.01$, ***$P < 0.001$, ****$P < 0.0001$, vs 0 group.

■ RESULTS AND DISCUSSION

Preparation of GEN Nanoparticles (GEN-NPs). An ROS scavenger, named TCD, was first synthesized by conjugating Tempol (TPL), a superoxide dismutase (SOD)-mimetic agent, onto β-cyclodextrin (β-CD). Briefly, TPL was first activated by 1,1-carbonyldiimidazole (CDI) and then chemically conjugated to the hydroxyl groups of β-CD (Figure S1, Supporting Information). The successful synthesis of TCD was demonstrated by Fourier transform infrared spectroscopy (FT-IR) and ^{1}H nuclear magnetic resonance (NMR) spectroscopy. As shown in the FT-IR spectrum (Figure S2A, Supporting Information), due to substitution of the hydroxyl groups, the absorption at 3410 cm^{-1} attenuated and a clear carbonyl signal appeared at 1750 cm^{-1}. Consistently, ^{1}H-NMR spectroscopy proved the

existence of a TPL moiety in the obtained TCD material, and proton signals from the methyl group of TPL were clearly observed (Figure S2B, Supporting Information). Because 4-(hydroxymethyl)phenylboronic acid pinacol ester (HMPBA-pin) can get rid of hydrogen peroxide (H_2O_2) and act as a catalase (CAT)-mimetic moiety,[30] HMPBA-pin-modified GEN (Gen-(HMPBA-pin)) was then synthesized (Figure S3A, Supporting Information). ^{1}H-NMR spectra (Figure S3B left panel, Supporting Information) clearly demonstrated the synthesis of Gen-(HMPBA-pin), as evidenced by the appearance of the carboxyl group. Electrospray ionization mass spectrometry (ESI-MS) (Figure S3C, Supporting Information) was used to determine the formation of the product Gen-(HMPBA-pin) (m/z 587.20) from GEN (m/z 271.06).
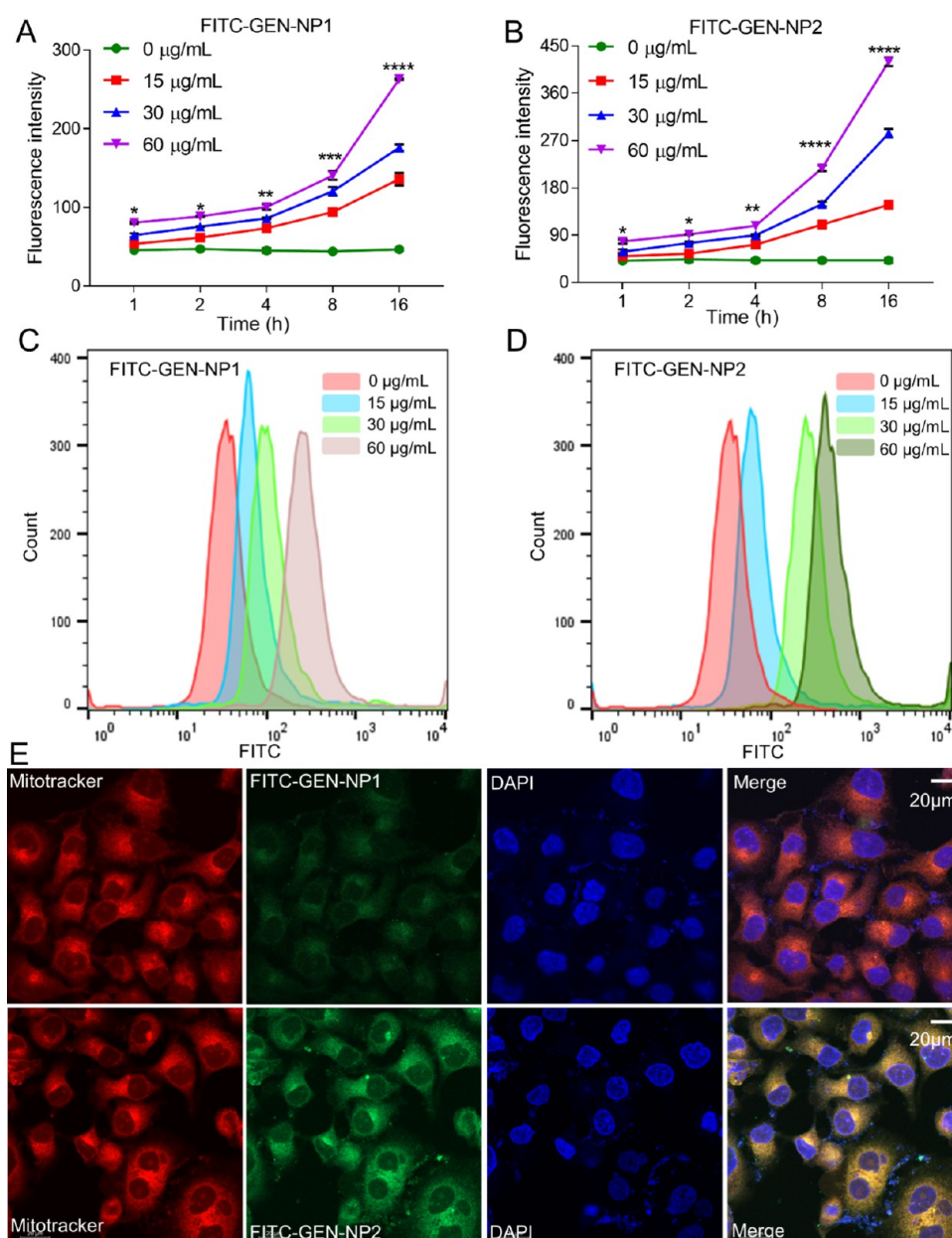
Figure 4. Cellular uptake of FITC-labeled GEN-NPs by colonic epithelial (NCM-460) cells. Quantification results of dose- and time-dependent cellular uptake of FITC-GEN-NP1 (A) and FITC-GEN-NP2 (B). Data are presented as the mean ± S.E.M. (n = 3). Typical flow cytometric curves of dose-dependent cellular uptake of FITC-GEN-NP1 (C) and FITC-GEN-NP2 (D) after 24 h of incubation with NCM-460 cells. (E) Fluorescence images showing colocalization of FITC/GEN-NPs with mitochondria in NCM-460 cells. For observation via confocal microscopy, nuclei were stained with DAPI (blue), while mitochondria were stained with MitoTracker (red). Scale bars, 20 μm. Data are shown as the mean ± S.E.M. (n = 3). Statistical significance was analyzed via two-way ANOVA with Dunnett's post hoc test for data in (A, B). *P < 0.05, **P < 0.01, ***P < 0.001, ****P < 0.0001, vs 0 μg/mL.

Combined with ^{13}C-NMR results (Figure S3B, right panel, Supporting Information), we confirmed that we synthesized monoesters of GEN, which were substituted in the 4′-OH position of GEN.[31] Finally, GEN or Gen-(HMPBA-pin) was encapsulated into TCD NPs using a nanoprecipitation/self-assembly method, and these GEN- or Gen-(HMPBA-pin)-containing TCD-derived nanoparticles were defined as GEN-NP1 or GEN-NP2, respectively (Figure S3D, Supporting Information). For GEN-NPs, D-α-tocopherol poly(ethylene glycol) 1000 succinate (TPGS) was used as a drug carrier.[32]

Successful preparation of GEN-NPs was verified by ^{1}H-NMR spectroscopy, FT-IR spectroscopy, and ultraviolet (UV)−vis

spectrophotometry (Figures 2A,B and S4A,B, Supporting Information). The FT-IR spectrum of GEN-NPs showed some characteristic peaks of GEN and TCD. The most prominent peak was at 3409 cm^{-1}, which represents the O−H stretching vibration. The aromatic C−H stretching vibration peak was observed at 2932 cm^{-1}. The vibrational stretching frequencies of C=O and C−O appeared at 1652 and 1032 cm^{-1}, respectively. Additionally, we observed a C−N stretching vibration at 1241 cm^{-1}. Scanning electron microscopy (SEM) and transmission electron microscopy (TEM) observations further revealed that GEN-NPs displayed a uniform rod-like morphology, which was different from the crystal shape of GEN

Figure 5. Biological effects of GEN-NPs in NCM-460 cells. The NCM-460 cells were incubated with medium or LPS/3% DSS for 4 h, followed by stimulation with different concentrations of GEN-NPs or other materials for 24 h. The cells treated with DMEM served as the normal control. (A, B) Flow cytometric analyses showing intracellular ROS generation with GEN-NPs and LPS/3% DSS. (C) H_2O_2 scavenging capabilities of different materials in NCM-460 cells. (D, E) Release of the IL-1β (D) and TNF-α (E) in the NCM-460 cells. Data are shown as the mean ± S.E.M. ($n = 3$). Statistical significance was evaluated by two-way ANOVA with Dunnett's post hoc test for data in (C−E). *$P < 0.05$, **$P < 0.01$, ***$P < 0.001$, vs DMEM. &$P < 0.05$, &&$P < 0.01$, &&&$P < 0.001$, &&&&$P < 0.0001$, vs LPS + 3% DSS.

and TCD (the left and middle panels of Figures 2C,D and S4C in the Supporting Information). Furthermore, differential scanning calorimetry (DSC) was used to determine the crystallinity and polymorphic behavior of GEN and TCD associated with the GEN-NPs. The DSC thermogram of GEN showed a characteristic endothermic peak at 303.1 °C, while that of TCD showed two endothermic peaks at 117.8 and 325.6 °C. The typical peaks of GEN (286.1 °C) and TCD (100.5 °C) were found in the physical mixture, which indicated that these compounds remained in their crystalline state in the mixture. However, no characteristic peak of GEN was detected in the lyophilized GEN-NPs (Figure S4D, Supporting Information). These results verified that GEN lost its crystalline state when

encapsulated in NPs. The mean diameters of GEN-NP1 and GEN-NP2 were 636 ± 94 and 304 ± 60 nm, respectively (the right panel of Figure 2C,D), which was consistent with the electron microscopy results. In addition, GEN-NP1 and GEN-NP2 had different ζ-potentials of −21.08 ± 1.51 and 6.63 ± 1.91 mV, respectively. Consistently, the ζ-potential of genistein-loaded nanostructured lipid carriers was −20.21 ± 2.4 mV.[33] The change in ζ-potential of GEN-NP2 may be due to the presence of HMPBA-pin.[34] The drug loading content efficiencies of GEN-NP1 and GEN-NP2 were 22.37 ± 0.28 and 33.11 ± 0.49%, respectively (Figure S4E,F, Supporting Information).

F

Hydrolysis Behaviors, Drug Release, and ROS-Scavenging Capability of GEN-NPs. Due to the ROS response characteristic of the TPL and HMPBA-pin moieties in TCD and Gen-(HMPBA-pin), GEN-NPs are hydrolyzable and release GEN when encountering ROS.[35] GEN-NPs incubated with 10 mM H_2O_2 showed a clear time-dependent hydrolysis curve (Figure 3A,B). Additionally, the rate of hydrolysis increased significantly with the increase of H_2O_2 concentration (Figure S5A,B, Supporting Information). Notably, GEN-NP1 showed a slower hydrolysis rate than GEN-NP2, indicating less GEN release (Figure 3A,B). Moreover, GEN-NP2 could effectively eliminate H_2O_2 in a dose−response pattern. In contrast, GEN-NP1 showed weaker H_2O_2 scavenging ability (Figure 3C). These results were in accord with the results of another study showing that the carbonate ester-linked HMPBA-pin was more sensitive to H_2O_2 than TPL.[35] An *in vitro* study was then performed to further confirm the ROS-scavenging capacity of GEN-NPs. First, the removal of a superoxide anion $(O_2^{\bullet-})$ by GEN-NPs showed a dose-dependent effect after incubation at 37 °C for 50 min (Figure 3D). Then, the free radical elimination capability of GEN-NPs was assessed using a 2,2-diphenyl-1-picrylhydrazyl (DPPH) assay.[36] As shown in Figure 3E,F, the DPPH radical was stable in the absence of GEN-NPs, and upon incubation with GEN-NPs, the time- and dose-dependent elimination curves were obtained. At 120 μg/mL GEN-NPs, 8 h of GEN-NP1 incubation resulted in nearly 75% scavenging of the DPPH radical (Figure 3E), while that for GEN-NP2 treatment was nearly 85% (Figure 3F). Collectively, these results substantiate the notion that GEN-NPs can eliminate a broad spectrum of ROS. Notably, compared with TPL, TCD, GEN, Gen-(HMPBA-pin), or TPGS alone, only GEN-NP2 efficiently scavenged all of the examined ROS (Figure S5C−E, Supporting Information).

Cellular Uptake and *In Vitro* Cytotoxicity Studies of GEN-NPs in Colonic Epithelial (NCM-460) Cells. The physical intestinal barrier comprises intestinal epithelial cells.[37] Key studies have demonstrated that the intestinal barrier damage precedes the clinical diagnosis of IBD. An aberrant increase of intestinal epithelial cell death is the characteristic of several intestinal diseases, such as IBD.[38] Accordingly, we examined the cellular internalization of GEN-NPs in colonic epithelial cells. After incubation with NCM-460 cells, FITC-labeled GEN-NP uptake was evaluated using a fluorescence microplate reader in combination with flow cytometry. The results showed that significant fluorescence could be found in cells after 60 min of incubation. With prolonged incubation, the fluorescence signals of GEN-NPs gradually increased. In addition, the results revealed dose-dependent cellular internalization of FITC/GEN-NPs (Figure 4A,B). Flow cytometry demonstrated gradually increased fluorescence signals in NCM-460 cells when the FITC/GEN-NP dose increased after incubation for 24 h (Figure 4C,D). Notably, the uptake of FITC-GEN-NP2 was higher than that of FITC-GEN-NP1 (Figure S6A, Supporting Information), possibly due to the NP properties, such as the shape,[39] small size, and positive ζ-potential.[40] ROS generation is well known to be a fundamental role of mitochondria.[41] We next investigated the intracellular trafficking of GEN-NPs in NCM-460 cells using confocal microscopy. In this experiment, the GEN-NPs showed the ability to target mitochondria, which overlapped completely with MitoTracker Red assay results. These findings further substantiated the ROS-responsive feature of GEN-NPs (Figure

4E). Overall, the GEN-NPs synthesized in this study can be rapidly and efficiently internalized by colonic epithelial cells.

Cellular toxicity analysis of GEN-NPs showed no obvious changes in cell viability after incubation with GEN-NPs or other materials at doses less than 60 μg/mL for 24 h (Figure S6B−H, Supporting Information). When the concentration of TPGS, TPL, or GEN reached 120 μg/mL, low cytotoxicity was observed in NCM-460 cells (Figure S6B−D, Supporting Information); however, for TCD, Gen-(HMPBA-pin), and GEN-NPs, the proportion of viable cells was still higher than 95% at this dose.

ROS-Scavenging, Antioxidative, and Anti-Inflammatory Effects of GEN-NPs in NCM-460 Cells. Abnormal ROS generation is a key mediator in the pathogenesis of inflammation. H_2O_2 is produced during the folding of oxidized proteins in the endoplasmic reticulum,[42] which favors Ca^{2+} release from the endoplasmic reticulum. The produced Ca^{2+} can lead to ROS production by disrupting the Mito-ETC. In turn, ROS promotes Ca^{2+} release from the endoplasmic reticulum. The oxidative stress elevation finally reached a toxic ROS threshold, leading to various inflammation-associated pathological changes.[43] Therefore, we explored whether GEN-NPs can restrain ROS production in NCM-460 cells. After stimulation with lipopolysaccharide (LPS) and 3% dextran sulfate sodium salt (DSS) for 24 h, NCM-460 cells exhibited a considerably high ROS level, which was probed with the fluorescent dye 2′,7′-dichlorofluorescein-diacetate (DCF-DA) (Figure 5A,B). In contrast, after the stimulated NCM-460 cells were treated with GEN-NPs for 24 h, the fluorescence signals of DCF-DA were significantly reduced, especially in GEN-NP2-treated cells (Figure 5A,B). Quantitative analysis using a fluorescence microplate reader further illustrated that the production of intracellular ROS in stimulated NCM-460 cells can be effectively suppressed by TPL, TCD, GEN-NP1, or GEN-NP2 (Figure S7A, Supporting Information). Because of the better permeability of the cell membrane to GEN-NP2, the ROS-scavenging ability of GEN-NP2 was comparable to that of TPL or TCD. Additionally, we determined the elimination of H_2O_2 by GEN-NPs. As expected, GEN-NP2 was able to scavenge H_2O_2 more effectively than TPL, TCD, or GEN-NP1 (Figure 5C), and cell viability increased correspondingly (Figure S7B−H, Supporting Information). Notably, GEN and Gen-(HMPBA-pin) showed lower ROS-scavenging capability than TPL or TCD in cells, which may be due to their poor water solubility and low bioavailability (Figures 5C and S7A, Supporting Information).

Anti-inflammatory therapeutics by targeting the excessive ROS accumulation to interrupt the aberrant inflammatory response has been studied for decades, which has been proven to be a feasible strategy for inflammation intervention. Therefore, we investigated whether GEN-NPs can alleviate inflammatory responses in intestinal epithelial cells. Treatment of NCM-460 cells with LPS/3% DSS obviously increased the secretion of interleukin-1β (IL-1β) and tumor necrosis factor-α (TNF-α) (Figure 5D,E). Coincubation with 60 or 30 μg/mL TPL, TCD, GEN-NP1, or GEN-NP2 for 24 h significantly reduced the release of these cytokines. In contrast, free GEN or Gen-(HMPBA-pin) showed no significant effects on IL-1β secretion or limited the effects on TNF-α levels. Our results verified that GEN-NPs can attenuate inflammation in intestinal epithelial cells and decrease intracellular ROS production.

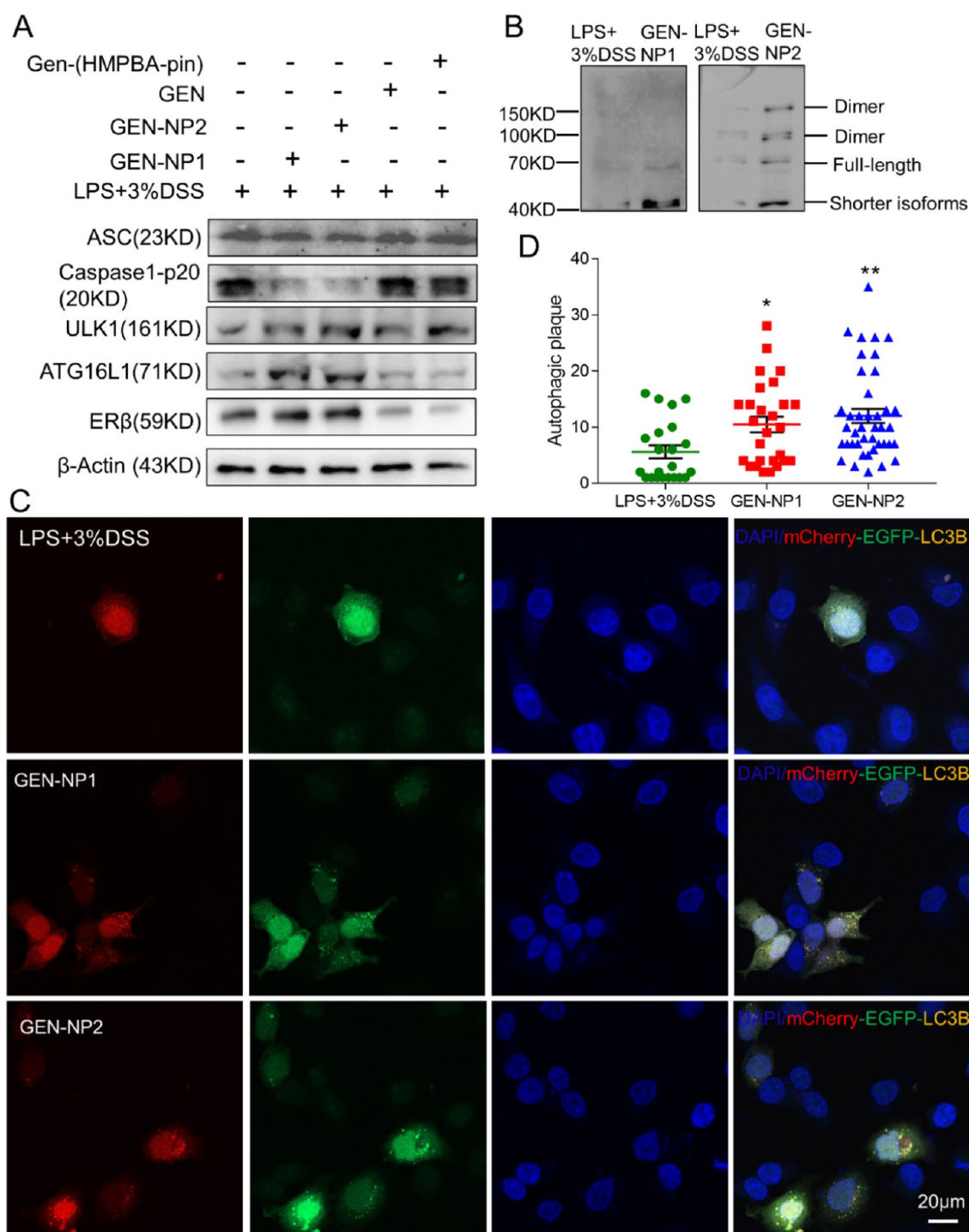**GEN-NPs Regulate the Autophagy-Inflammasome Signaling Pathway in NCM-460 Cells via Estrogen**

Figure 6. GEN-NPs regulate the autophagy-inflammasome signaling pathway in NCM-460 cells. NCM-460 cells were incubated with LPS/3% DSS for 4 h, followed by treatment with or without 30 μg/mL GEN-NPs for 24 h. (A) The expression levels of ASC, Caspase1-p20, ULK1, ATG16L1, and ERβ analyzed using western blot. (B) Detection of ERβ dimerization. (C) Confocal microscopy images showing EGFP-mCherry-LC3B (yellow) expression in treated NCM-460 cells (Scale bars, 20 μm). (D) Changes in cells containing autophagy-related puncta were calculated from at least 10 areas (400 cells) of interest pooled from three independent experiments. Data are shown as the mean $\pm$ S.E.M. (n = 3). Statistical significance was evaluated by one-way ANOVA with Tukey's post hoc analysis for the data in (D). *$P < 0.05$, **$P < 0.01$, vs LPS + 3% DSS.

Receptor β (ERβ) Activation. Inflammasomes are core participants in pathogens' innate immunity, and their role in intestinal epithelial cells (IECs) has received great attention. Inflammasomes contain a set of heterogeneous cytosolic multiprotein complexes whose function is to detect infectious or harmful stimuli and act as a platform to activate specific proinflammatory caspase proteases, the most well known of which is Caspase 1. Inflammasomes proteolytically activate IL-1β and cause its secretion along with other proinflammatory cytokines. Inflammasomes have been implicated in IBD progression.[44] Therefore, we detected inflammasome complex apoptosis-associated speck-like protein containing a CARD (ASC) and Caspase1-p20 expression after incubation with GEN-NPs. The results showed that although they had limited
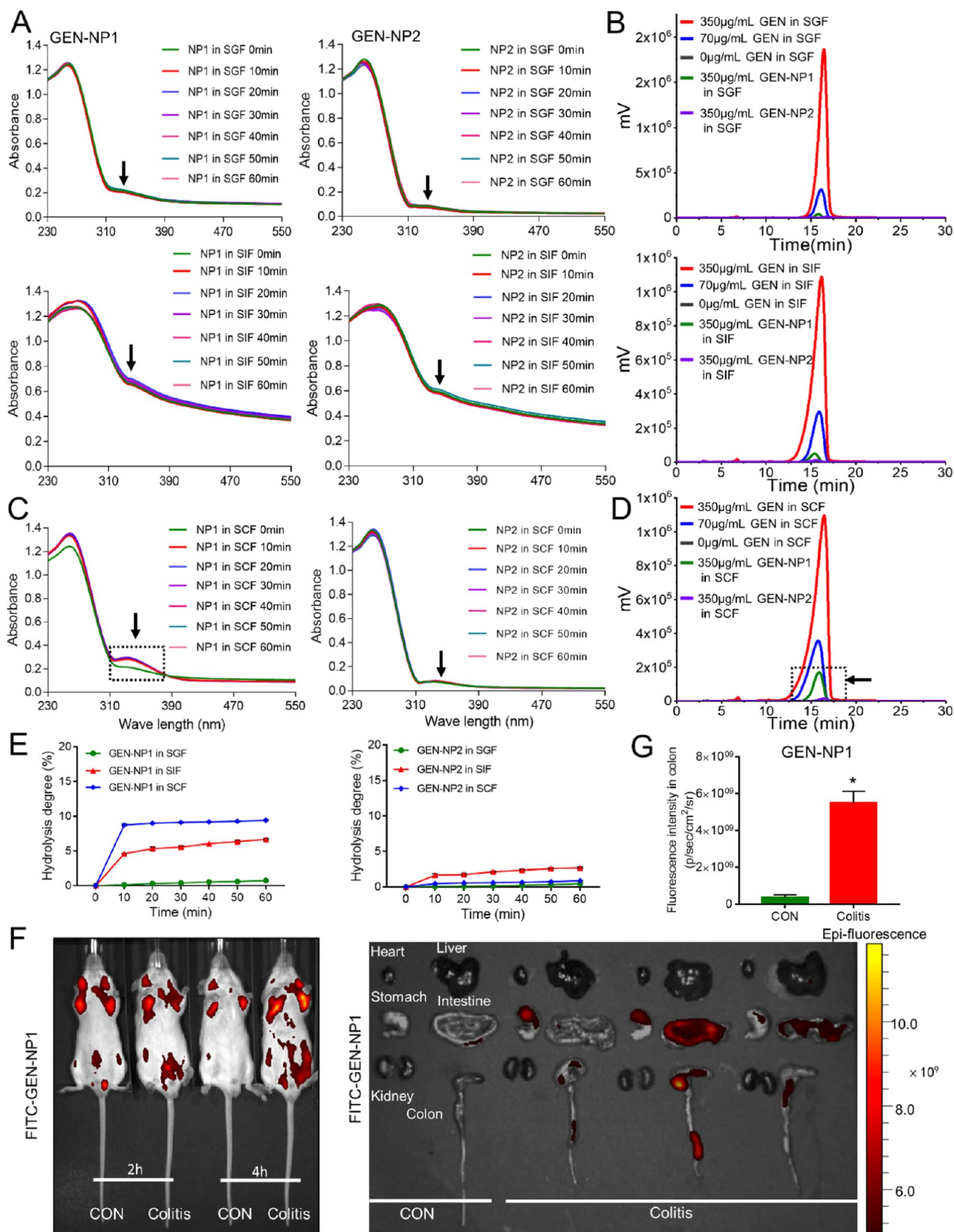
Figure 7. GEN-NPs preferentially localize to the inflamed colon. (A−D) Detection of chemical stability of GEN-NPs in SGF, SIF, and SCF via ultraviolet−visible spectroscopy (A, C) and HPLC (B, D). (E) Drug release curves of GEN from GEN-NPs in different simulated buffer solutions. (F) Biodistribution analysis of FITC-labeled GEN-NP1 in healthy or 3% DSS-induced colitis mice using *ex vivo* imaging. (G) Quantification of the FITC-GEN-NP1 fluorescence signal in the colon. Student's *t*-test was employed for analysis of the data in (G). Data are shown as the mean ± S.E.M. ($n = 3$). *$P < 0.05$, vs CON.
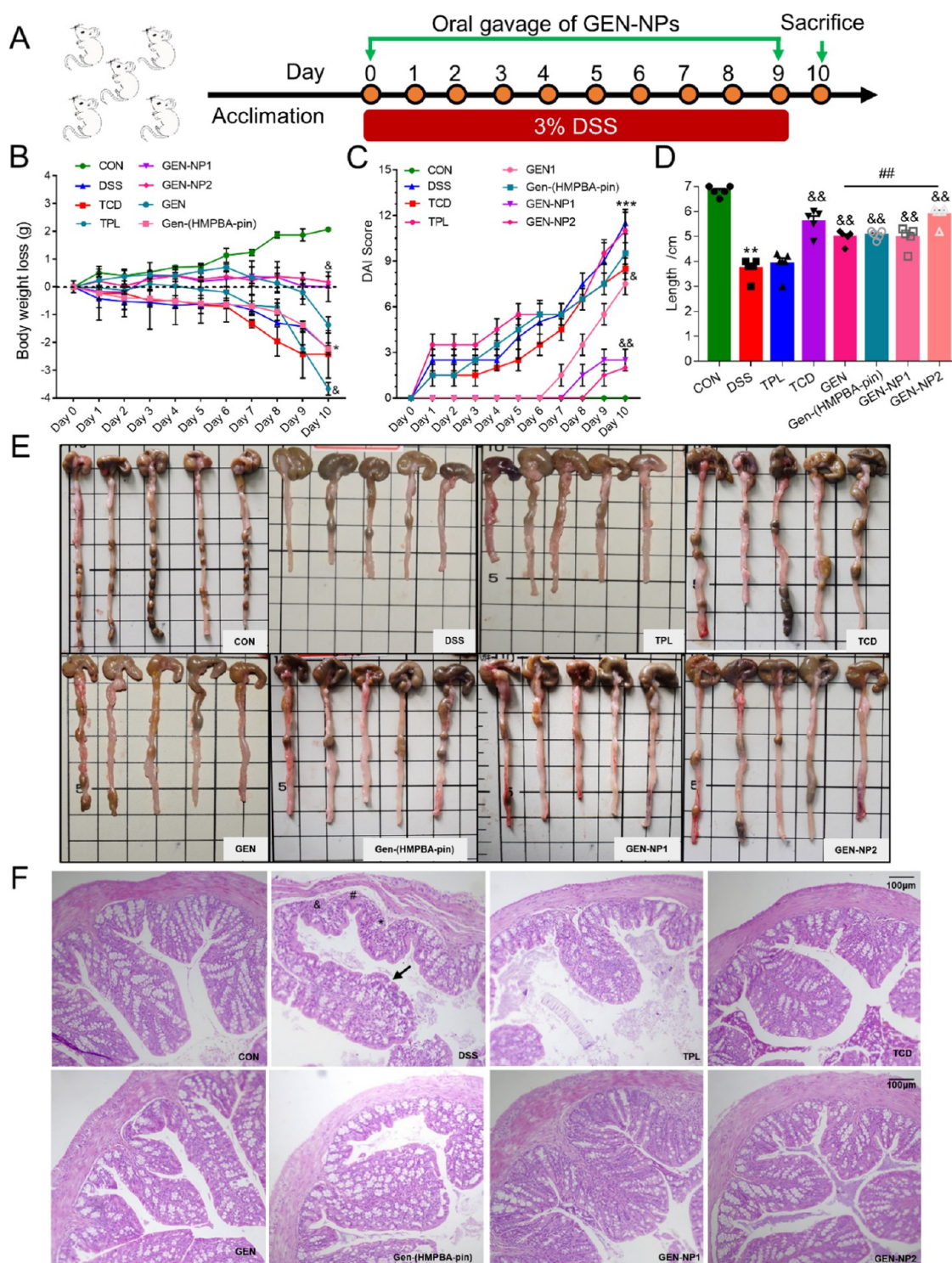
Figure 8. Treatment of GEN-NPs on acute colitis. (A) Illustration of treatment regimens. (B) Weight loss of treated mice. (C) Changes in DAI. Data are shown as the mean ± S.E.M. ($n = 5$). Statistical significance was analyzed via two-way ANOVA with Dunnett's post hoc test for data in (B, C). *$P <$ 0.05, ***$P < 0.001$, vs CON; &$P < 0.05$, &&$P < 0.01$, vs DSS. (D, E) Quantified lengths (D) and representative digital photos (E) of colonic tissues isolated from mice. Statistical significance was evaluated via one-way ANOVA with Tukey's post hoc analysis for the data in (D). **$P < 0.01$, vs CON; &&$P < 0.01$, vs DSS, ##$P < 0.01$, vs GEN-NP2. (F) HE staining of distal colon sections obtained from mice given water (CON), DSS (DSS), or different drugs and assessed on day 10. Note the epithelial disruption (arrow), crypt destruction (#), goblet cell depletion (*), and significant granulocyte infiltration (&) in DSS-treated mice.

effects on ASC expression, GEN-NPs could significantly inhibit Caspase1-p20 expression (Figures 6A and S8A, Supporting Information), which indicated that GEN-NPs help cells avoid inflammasome activation to inhibit cytokine release.

Previous studies have confirmed the relationship between CD and autophagosomes. The autophagosome membrane formation protein autophagy-related 16 like 1 (ATG16L1) regulates inflammasome activation and prevents necroptosis or Paneth
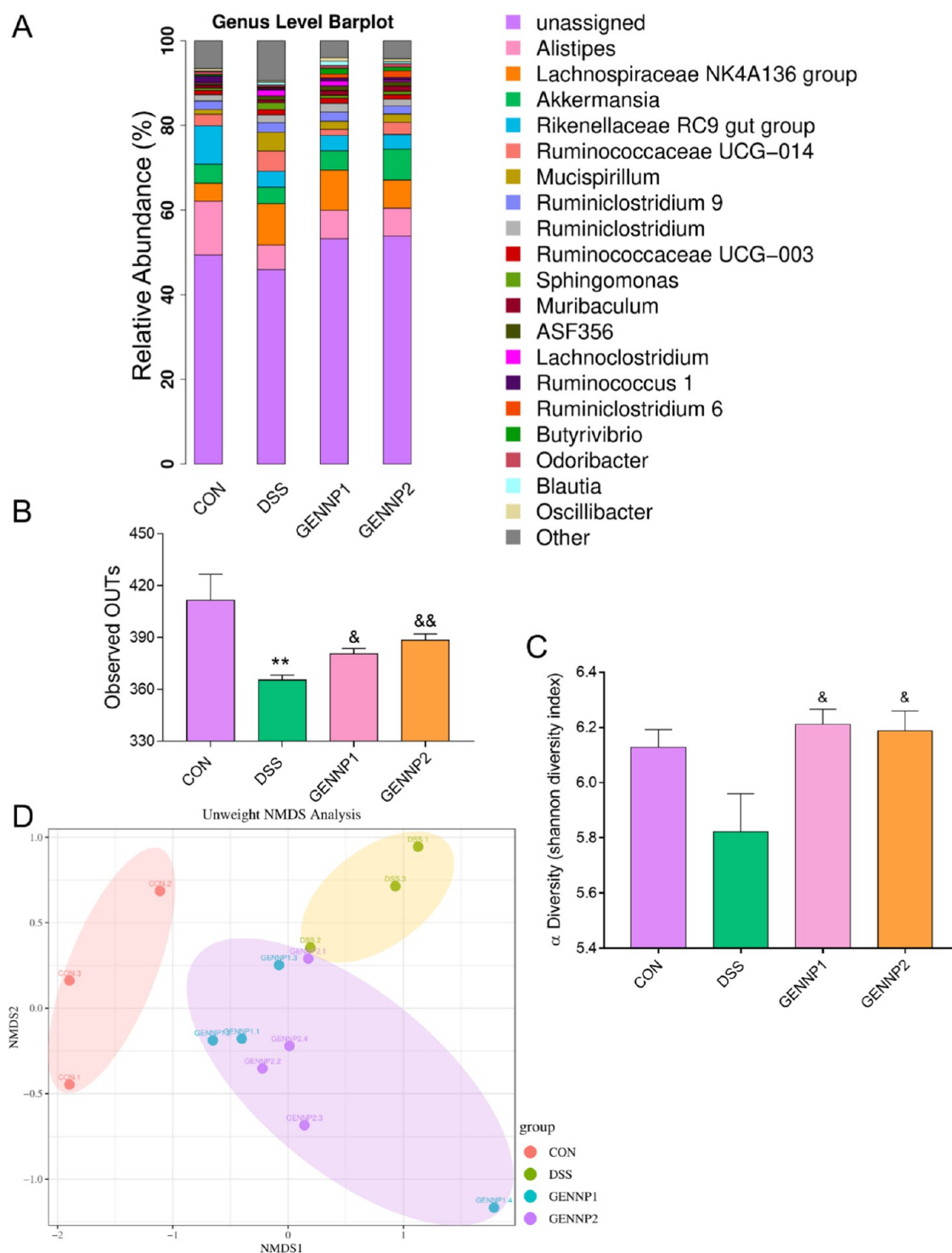
Figure 9. Regulation of oxidative stress and inflammation by GEN-NPs. (A, B) Levels of H_2O_2 and MDA. (C, D) Release of TNF-α and IL-1β in colonic tissues. (E, F) Antioxidase activities of CAT and SOD. (G) Levels of MPO, an abundant hemoprotein present in neutrophils and monocytes. Data are shown as the mean $\pm$ S.E.M. ($n = 5$). Statistical significance was analyzed via one-way ANOVA with Tukey's post hoc analysis. *$P < 0.05$, **$P < 0.01$, vs CON and &$P < 0.05$, &&$P < 0.01$, &&&$P < 0.001$, vs DSS.

cell loss.[45] To elucidate the regulatory mechanism of GEN-NPs on inflammasome activation, we investigated changes in ATG16L1 and unc-51-like autophagy activating kinase 1 (ULK1) levels, the initiator of autophagy. As demonstrated in Figures 6A and S8A, a remarkable increase in autophagy-related protein expression was observed.

ERβ activation after GEN and GEN-NP treatment was then investigated. Due to its estradiol-like structure, GEN can initiate signal transduction by interacting with the estrogen receptor (ER),[46] which, upon ligand binding, dimerizes and translocates to the nucleus to regulate the transcription of many genes, thus modulating critical physiologic processes, including colon inflammation and the intestinal epithelial barrier.[47−49] More importantly, ERβ has been found to regulate autophagy in breast

cancer cells,[50] SH-SY5Y cells,[51] and colon cells.[52] In our study, GEN-NPs significantly promoted the expression and dimerization of ERβ, the predominantly expressed ER isotype in the colon. Full-length or shorter isoforms of ERβ were observed in GEN-NP-treated NCM-460 cells, suggesting that GEN-NPs improve autophagy by affecting ERβ (Figures 4A,B and S8B, Supporting Information).

To further investigate how GEN-NPs affect autophagic flux during inflammation, we examined autophagy-associated protein light chain 3B (LC3B) trafficking using confocal microscopy. Briefly, we expressed EGFP-mCherry-LC3B in NCM-460 cells to visualize the transition of LC3B from autophagosomes to autolysosomes. EGFP-mCherry-LC3B appears yellow in neutral autophagosomes but red in acidic

Figure 10. Regulation of gut microbiota by GEN-NPs. (A) Changes at the genus level in fecal microbiota composition. (B) Gut microbiota α diversity (observed OTUs) in different treatment groups. (C) Shannon α diversity of the microbial community in different treatment groups. (D) NMDS analysis of the microbiota composition in representative samples. Data are shown as the mean $\pm$ S.E.M. (n = 3 or 4). Statistical significance was evaluated via one-way ANOVA with Tukey's post hoc analysis for data in (B, C). **$P < 0.01$, vs CON and $^{\&}P < 0.05$, $^{\&\&}P < 0.01$, vs DSS.

autolysosomes due to quenching of GFP. EGFP-mCherry-LC3B showed low and diffuse cytoplasmic expression in NCM-460 cells treated with LPS/3% DSS, suggesting that autophagy was inhibited. In contrast, EGFP-mCherry-LC3B showed high and punctate expression in NCM-460 cells treated with GEN-NPs, suggesting that autophagy was restored (Figure 6C,D). Stimulation with GEN-NP2 appeared to facilitate autophagic flux in cells, indicated by an increase in the number of

autolysosomes (Figure 6C). These results suggest that GEN-NPs can regulate the autophagy-inflammasome signaling pathway to exert anti-inflammatory activity via ERβ activation.

GEN-NPs Preferentially Localize to the Inflamed Colon. To test whether GEN-NPs can survive the harsh gastrointestinal tract environment and can be plentifully delivered to the colon to exert an anti-inflammatory therapeutic effect against IBD, we incubated GEN-NPs with simulated

gastric, intestinal, or colonic fluids (SGF, SIF, or SCF) for 1 h at 37 °C. The GEN released from GEN-NPs was analyzed via UV−visible spectroscopy and high-performance liquid chromatography (HPLC). As expected, GEN-NPs were stable in the simulated gastric and intestinal digestive juice (Figure 7A,B). In contrast, GEN-NP1 displayed an obvious hydrolysis profile in SCF (Figure 7C,D). The drug release curves of GEN from GEN-NPs in different simulated buffer solutions showed that only a small portion of GEN (1−10%) could be released within 20 min (Figure 7E). We further confirmed the results using gastric/colonic contents (GC/CC), and similar results were obtained (Figure S9A−D, Supporting Information).

The mucosal ROS concentration in patients suffering from IBD has been reported to be 10−100 times higher than that in normal patients. Thus, the SOD and CAT mimetic components TPL and HMPBA-pin in GEN-NPs can effectively respond to and scavenge excess ROS in the inflamed colon. The biodistribution of FITC-labeled GEN-NPs in acute colitis model mice after oral administration at different time points was recorded. As shown by *ex vivo* imaging, negligible fluorescence in the colon of healthy mice indicated that little GEN-NPs were accumulated in this tissue. In contrast, the FITC-labeled GEN-NPs were clearly localized to the inflamed colon (Figures 7F and S9E, Supporting Information). Notably, GEN-NPs were almost completely metabolized after 4 h of treatment in normal mice. This suggests that GEN-NPs will not induce cumulative toxicity. However, GEN-NPs remained longer in the inflamed tissues, which is beneficial to targeted therapy. Additionally, quantification of the fluorescence signal in the colon indicated that FITC-labeled GEN-NP2 had significantly stronger fluorescence signals in colons from colitis mice than in colons from FITC-labeled GEN-NP1-treated mice (Figures 7G and S9F, Supporting Information). This can be attributed to GEN-NP1 displaying a hydrolysis profile in SCF or CC. These results suggest that GEN-NPs can accumulate at the site of inflammation for a long time and exert their therapeutic efficacy through scavenging ROS.

Therapeutic Effects of GEN-NPs in Acute Colitis. We then evaluated the therapeutic efficacy of GEN-NPs in an acute colitis mouse model. Male, eight-week-old BALB/c mice were used as follows: (i) control group (CON group); (ii) colitis model group induced with 3% DSS (DSS group); (iii) colitis model group treated with TPL (1 mg/mL, 200 μL/day) (TPL group); (iv) colitis model group treated with TCD (1 mg/mL, 200 μL/day) (TCD group); (v) colitis model group treated with GEN (1 mg/mL, 200 μL/day) (GEN group), (vi) colitis model group treated with Gen-(HMPBA-pin) (1 mg/mL, 200 μL/day) (Gen-(HMPBA-pin) group); (vii) colitis model group treated with GEN-NP1 (0.05 mg/mL, 200 μL/day) (GEN-NP1 group); and (viii) colitis model group treated with GEN-NP2 (0.05 mg/mL, 200 μL/day) (GEN-NP2 group) (Figure 8A). On day 10, GEN-NP2 showed excellent therapeutic effects against colitis. The mice in the GEN-NP2 group had less weight loss, a lower disease activity index (DAI), and a longer colon length than the DSS group (Figure 8B−E). Histological analysis showed that mice with DSS-induced colitis mice showed notable damage in the colon, with epithelial disruption, crypt destruction, goblet cell depletion, and obvious granulocyte infiltration. However, the histological microstructure in the GEN-NP2 treatment group revealed an intact epithelium and normal crypts with neatly arranged goblet cells (Figure 8F). Although used at a higher concentration, TCD, GEN, and Gen-(HMPBA-pin) offered lower efficacies than GEN-NP2 (Figure

8B−F). In addition, oral administration of TPL, TCD, GEN, Gen-(HMPBA-pin), GEN-NP1, and GEN-NP2 showed no hepatoxicity (Figure S10, Supporting Information).

Regulation of Oxidative Stress, Inflammation, and Gut Microbiota by GEN-NPs. Subsequently, the *in vivo* effects of GEN-NPs on oxidative stress and inflammation were examined. As shown in Figure 9A−D, GEN-NP2 obviously reduced the levels of H_2O_2, malondialdehyde (MDA), TNF-α, and IL-1β, indicating that both oxidative stress and inflammatory responses were mitigated. Similarly, the mice treated with GEN-NP2 displayed the highest CAT and SOD antioxidant activities and the lowest myeloperoxidase (MPO) content (Figure 9E−G). In comparison, TCD, TPL, GEN, Gen-(HMPBA-pin), and GEN-NP1 partially reduced the generation of oxidative stress and inflammation. The satisfactory efficacy of GEN-NP2 may be attributed to its regulation of the autophagy-inflammasome pathway via ERβ activation (Figure S11A,B, Supporting Information).

Increasing evidence indicates that the imbalance of gut microbiota is closely related to the pathogenesis of colitis.[53] Therefore, we investigated the gut microbiota composition in GEN-NP-treated mice using 16S rRNA gene sequencing. Compared to healthy mice, colitis mice showed a decreased proportion of *Alistipes*, which exhibit protective effects against colitis.[54,55] Additionally, samples from the DSS group demonstrated an increase in the *Lachnospiraceae_N-K4A136_group*, a major bacterial taxon with an average relative abundance of over 10% in colitis mice.[56,57] In contrast, only GEN-NP2 treatment reduced the expansion of the *Lachnospiraceae_NK4A136_group* and increased *Alistipes* levels (Figures 10A and S11C, Supporting Information). Importantly, GEN-NP2 treatment increased the levels of the "famous" gut microbiota *Akkermansia*, which is well known for modulating energy metabolism, glucose tolerance, and immune system function.[58] Because of the modulations of these gut microbiota, there was a decrease in inflammation in GEN-NP2-treated mice.[59]

The observed OTUs, a quantitative measure of species richness, demonstrated that the DSS group had a drop in community richness. In contrast, GEN-NPs had an impact on taxon richness, as the GEN-NP1 and GEN-NP2 groups had an increased number of observed OTUs (Figures 10B and S11D, Supporting Information). We also analyzed the Shannon diversity index, an indicator of community diversity. As shown in Figure 10C, there was parallel community diversity between the CON and GEN-NP groups. However, significant differences were found in the Shannon index between the GEN-NP and DSS groups, suggesting that GEN-NP significantly improved the diversity of the microbiota. Furthermore, the nonmetric multidimensional scaling (NMDS) plot of unweighted UniFrac distance showed a clear difference in the phylogenetic structure of fecal bacteria between the DSS treatment group and the control group (Figure 10D). Notably, the similar fecal microbiota in the GEN-NP-treated mice could be due to the probiotic role of GEN,[60−62] which, as a polyphenol, can influence the gut microbiota composition.[59] These results prove that GEN-NP treatment can restore the microbial community of mice with colitis.

■ CONCLUSIONS

In summary, we synthesized an ROS-responsive GEN-derived nanomaterial named GEN-NP2, which is a promising nanomedicine for the treatment of IBD without accompanying

toxicity. GEN-NP2 was found to passively target the inflamed colon, effectively scavenge ROS, regulate the inflammasome-autophagy pathway, and influence the gut microbiota composition, thereby promoting the recovery of colonic inflammation. Furthermore, unlike the parent GEN, GEN-NP2 showed obviously improved bioavailability and tissue-targeting ability for inflammation, which can expand its use to other oxidative stress-, inflammation-, or damage-related diseases. Therefore, this work not only emphasizes the potential of using GEN-NPs as an ideal drug for IBD but also provides insights into how GEN-NPs exert their anti-inflammatory effects.

■ MATERIALS AND METHODS

Materials. TPL, β-CD, CDI, 4-dimethylaminopyridine (DMAP), anhydrous dichloromethane (DCM), HMPBA-Pin, succinic anhydride, pyridine, tetrahydrofuran (THF), N,N'-diisopropylcarbodiimide (DIC), dichloromethane (DCM), GEN, TPGS, and DPPH were provided by Macklin (China). FITC was purchased from YEASEN (China).

Synthesis of TCD. TCD was prepared according to a previous study.[63] Firstly, TPL was activated by CDI. Subsequently, dissolving CDI-activated TPL (0.825 g) with anhydrous DMSO (10 mL), and then, β-CD (1.175 g, 1.035 mmol) and DMAP (0.565 g, 4.65 mmol) were added under nitrogen. After stirring for 24 h at 25 °C, the final product was precipitated from a mixed solution of diethyl ether and methanol (1:1, v/v). Finally, a pink powder (TCD) was obtained via centrifugation and lyophilization.

Characterization of TCD. TCD was characterized using ^{1}H-NMR (Bruker Biospin Inc., AVANCE III HD system), FT-IR (Thermo Fisher Scientific, Nicolet iS5 FT-IR spectrometer), and UV−vis (Shimadzu, UV-2600 spectrophotometer) spectrometry.

Synthesis of Gen-(HMPBA-pin). First, HMPBA-Pin-SA was synthesized in line with a previous study.[64] GEN (660 mg, 2.47 mmol) was dissolved in 10 mL of dichloromethane, and then HMPBA-pin-SA (3.6 g, 10.8 mmol), DMAP (30 mg, 0.267 mmol), and DIC (1.56 mL, 10.8 mmol) were added. The obtained mixture was mixed for 24 h at room temperature. Finally, the crude product was purified via solid-phase extraction.

^{1}H- and ^{13}C-NMR spectra and mass spectrometry were used to characterize Gen-(HMPBA-pin). MS analysis was performed using G2-XS QTof (Waters) equipment. Briefly, 2 μL of GEN or Gen-(HMPBA-pin) was injected into a UPLC column (ACQUITY UPLC BEH C18 column, 2.1 × 10 mm^2). Water containing 0.1% formic acid and acetonitrile containing 0.1% formic acid were used as eluents A and B, respectively. The elution gradient was 5% eluent B for 0.5 min, 5−95% eluent B for 11 min, and 95% eluent B for 2 min. MS analyses were conducted using an ESI source, positive ion mode, and MS acquisition mode (mass range: 100−1200 m/z; capillary voltage: 2.5 kV; cone voltage: 40 V; source temperature: 120 °C; desolvation gas temperature: 800 °C). Leucine-enkephalin, as a lock mass, was used for recalibration. Acquired data were processed via Masslynx 4.1 software.

Preparation of GEN-NPs. A total of 10 mg of TPGS, 10 mg of TCD, and 10 mg of GEN were dissolved in 10 mL of 1,4-dioxane solvent. After stirring at 25 °C for 20 min, 20 mL of water was added within 1 h, and then 70 mL of water was injected within another 1 h. In the above operation, the stirring speed was fixed at 1000 rpm, and the temperature was fixed at 25 °C. The product was stirred for an additional 24 h, and then dialysis (MW, 500 Da) was performed to remove organic solvents. The final assembled product (GEN-NP1, 3 mg) was harvested by freeze-drying. In the same way, nanoparticles containing Gen-(HMPBA-pin) (GEN-NP2, 6 mg) and FITC-labeled GEN-NPs were prepared.

Characterization of GEN-NPs. Malvern Zetasizer Nano ZS instrument was used to quantify the size distribution curves and ζ-potential of GEN-NPs at room temperature. TEM was performed using an H-7650 microscope (Hitachi, Japan). SEM was conducted with a JSM-7600F microscope (JEOL, Japan).

The state of GEN in the NP formulation was determined using DSC. The samples (GEN, TCD, physical mixture, and GEN-NPs) were analyzed with a DSC1 differential scanning calorimeter (METTLER TOLEDO, Switzerland). Al_2O_3 was used as a reference to determine the baseline. During the scanning process, a heating rate of 5 °C/min was set to range from 40 to 340 °C.

The loading GEN (W_1) content in different GEN-NP1 samples was determined by UV−vis spectrometry of GEN. To this end, GEN was extracted from an aqueous solution of GEN-NP1 (3 mg) using a hypothermal ultracentrifugation method. Then, the concentration of GEN was quantified via UV−vis spectrometry. The detection wavelength was set at 350 nm. Encapsulation efficiency and drug loading were obtained via eqs 1 and 2, respectively.

$$\text{encapsulation efficiency} = (3 - W_1)/3 \times 100\% \tag{1}$$

$$\text{drug loading} = (3 - W_1)/10 \times 100\% \tag{2}$$

Through similar procedures, the GEN-NP2 (6 mg) encapsulation efficiency and drug loading were detected.

Hydrolysis of GEN-NPs and Drug Release in the Presence of H_2O_2. After GEN-NPs (1 mg/mL) were incubated with PBS (0.01 M, pH 7.4) containing different concentrations of H_2O_2, the drug release and degree of hydrolysis were calculated according to the transmittance values, which were measured with a UV−vis spectrophotometer at 350 nm. The transmittance values at various time points were also obtained to calculate the hydrolysis degree. To characterize changes in the size and morphology of GEN-NPs, the corresponding samples were characterized via TEM/SEM and with a Malvern Zetasizer Nano ZS instrument.

Stability of GEN-NPs in Physiological Fluids. The stability of GEN-NPs in fluids simulating the alimentary tract environment was examined. For this purpose, GEN-NPs were incubated in commercial simulated gastric fluid with pH 1.2 for 1 h, simulated intestinal fluid with pH 6.8 for 1 h, or simulated colonic fluid with pH 7.8 for 1 h. Then, the dissolution media were examined via UV−vis spectrometry and nanoparticle size analysis.

Additionally, murine gastric and intestinal contents were obtained for GEN-NP stability tests. Briefly, BALB/c mice were euthanized, and the entire stomach and colon tissues were washed separately with 7 mL of prechilled PBS. The supernatant was collected after centrifugation. Subsequently, 400 μL of GEN-NPs was incubated at 37 °C for 1 h in 800 μL of murine gastric and colonic contents.

GEN content was quantified via HPLC. A Shimadzu Prominence LC-20A system equipped with a Diamonsil C18 column (150 × 4.6 mm^2) and a Prominence SPD-M20A PDA detector (detection wavelength: 260 nm) was used. The mobile phase contained water and methanol (45:55, v/v).

ROS-Scavenging Capability of GEN-NPs. The ROS-scavenging capacity of GEN-NPs was assessed using the H_2O_2 assay kit (A064-1-1, Nanjing Jiancheng), inhibition and production superoxide anion assay kit (A052-1-1, Nanjing Jiancheng), and fresh solution of DPPH$^\bullet$ according to the previous study.[35]

Cell Line. NCM-460 cell was obtained from INCELL and cultured in Dulbecco's modified Eagle's medium (DMEM) (no phenol red, 21063029, Thermo Fisher Scientific) supplemented with 10% (v/v) charcoal-stripped fetal bovine serum (12676029, Gibco) and 1% (v/v) penicillin−streptomycin (1 mg/mL).

Analysis of Cellular Uptake of GEN-NPs. To quantify internalization of GEN-NPs, NCM-460 cells were seeded in a 6-well plate at an appropriate density, followed by the addition of different doses of FITC-labeled GEN-NPs. The fluorescence intensities were detected with a multifunctional fluorescence microplate reader (Infinite M200 PRO, TECAN). Finally, the fluorescence intensities of the digested cells were detected using flow cytometry (FACSCalibur, Becton Dickinson).

NCM-460 cells were seeded in 22 mm confocal dishes at a density of 2.0×10^5 cells per dish. After incubation with FITC-labeled GEN-NPs (60 μg/mL) for 24 h, the cells were incubated with 250 nM MitoTracker Red CMXRos Mitochondrial Probe (40741ES50, YEASEN) for 30 min at 37 °C. Then, the cells were fixed with 4%

paraformaldehyde and stained with 4′,6-diamidino-2-phenylindole (DAPI). The fluorescence signals were observed via ultrahigh-resolution confocal microscopy (LSM800, Zeiss).

Cell Activity Evaluation. NCM-460 cells seeded in 96-well culture plates were treated with GEN-NPs at different doses for 24 h to determine the toxicity of the synthesized particles. Cell activity was tested according to the Cell Counting Kit-8 (CCK-8) (40203ES76, YEASEN) protocol.

To determinate the effect of GEN-NPs on DSS-induced cell cytotoxicity, NCM-460 cells were first primed with LPS (100 ng/mL) for 4 h, and then with 3% (w/v) DSS (MB5535-2, Meilunbio) for 12 h prior to treatment with GEN-NPs for 24 h. The absorbance was obtained at 450 nm (BioTek).

Antioxidative Stress Effect of GEN-NPs in NCM-460 Cells. NCM-460 cells were cultured in 6-well plates at 2.0×10^6 cells per well. After cells were pretreated with LPS and 3% DSS for 12 h, they were stimulated with GEN-NPs for 24 h. Subsequently, the ROS levels of cells were detected using 2′,7′-dichlorodihydrofluorescein-diacetate (DCFH-DA, D6470, Solarbio). Intracellular fluorescence signals of DCF-DA were measured via flow cytometry and analyzed using FlowJo software.

Additionally, the H_2O_2-scavenging capacity of GEN-NPs in NCM-460 cells was also evaluated by the abovementioned method.

Anti-Inflammatory Effect of GEN-NPs in NCM-460 Cells. NCM-460 cells were cultured in 96-well plates at 1.0×10^4 cells per well. After cells were pretreated with LPS and 3% DSS for 12 h, they were stimulated with various doses of GEN-NPs for 24 h. The release of IL-1β and TNF-α in the culture supernatant was detected via ELISAs (Ml037301 and Ml028611, Mlbio), while the total protein levels were quantified by the BCA method (20201ES76, YEASEN).

Western Blotting Analysis. NCM-460 cells were cultured in 6-well plates at 2.0×10^6 cells per well. After cells were pretreated with LPS and 3% DSS for 12 h, they were stimulated with GEN or GEN-NPs for 24 h. NP-40 was used to collect proteins. After SDS-PAGE, proteins were blotted onto a 0.45 μm PVDF membrane. Primary antibodies were incubated with the PVDF membrane. Then, HRP-goat anti-mouse IgG (ab205719, Abcam) and HRP-goat anti-rabbit IgG (ab205718, Abcam) were applied. Alliance Q9 (UVItec, U.K.) was used to visualize chemoluminescence. The band analysis was performed via ImageJ software 1.51j8.

pmCherry-EGFP-LC3B Assay. The cells were transfected with pmCherry-EGFP-LC3B (PVT10398, Life Science Market) according to the protocol, followed by treatment with LPS and 3% DSS for 12 h and GEN-NPs for 24 h. The cells were fixed with 4% paraformaldehyde for 30 min at 37 °C and then counterstained with DAPI. The signals were observed by confocal immunofluorescence microscopy.

Animals. Animal experiments were carried out in strict accordance with the guidelines issued by Nanjing Agricultural University (License Number: SYXK (Su) 2017-0007). The male BALB/c mice (20−22 g) used in this study were obtained from GemPharmatech Bio. Co. (Nanjing, China). We randomly chose mice from the same or different littermates for the experimental group. All mice were provided with a normal diet and allowed to drink tap water *ad libitum*.

Animal Models of Colitis. After 7 days of acclimatization, colitis was induced using 3% DSS (36 000−50 000 MW) dissolved in drinking water, given *ad libitum* for 9 consecutive days. A previous study found that a 10 mg/kg body weight dose of GEN was more efficacious in ameliorating DSS-induced colitis.[18] Thus, we chose this dose in the present study. To identify the effects of GEN-NPs on colitis, mice were grouped as follows: (i) control group (CON group); (ii) colitis model group induced with 3% DSS (DSS group); (iii) colitis model group treated with TPL (1 mg/mL, 200 μL/day) (TPL group); (iv) colitis model group treated with TCD (1 mg/mL, 200 μL/day) (TCD group); (v) colitis model group treated with GEN (1 mg/mL, 200 μL/day) (GEN group), (vi) colitis model group treated with Gen-(HMPBA-pin) (1 mg/mL, 200 μL/day) (Gen-(HMPBA-pin) group); (vii) colitis model group treated with GEN-NP1 (0.05 mg/mL, 200 μL/day) (GEN-NP1 group); and (viii) colitis model group treated with GEN-NP2 (0.05 mg/mL, 200 μL/day) (GEN-NP2 group) (Figure 8A). Mice in different groups were administered different drugs by oral

gavage throughout the entire study period. The DAI was scored based on the average of five parameters: stool consistency, weight loss, rectal bleeding, food and water intake, and the mental state of the mice. The following scoring systems were applied. For stool consistency: well-formed pellets = 0, slightly soft = 1, very soft = 2, watery diarrhea = 3; for weight loss, none = 0, mild loss (1−5%) = 1, moderate loss (5−10%) = 2, severe loss (>10%) = 3; for rectal bleeding: no blood = 0, hemoccult positive = 1, visible blood traces in stool = 2, gross rectal bleeding = 3; for appetite: normal = 0, slightly change = 1, moderately change = 2, severely change = 3; and for attitude/activity: normal = 0, slightly change = 1, moderately change = 2, severely change = 3.

Biodistribution of GEN-NPs in Acute Colitis Mice. FITC-labeled GEN-NPs (0.05 mg/mL, 200 μL) were used to evaluate the localization and biodistribution of GEN-NPs in acute colitis mice. *Ex vivo* imaging was conducted via a living imaging system (IVIS Spectrum, PerkinElmer).

Necropsy, Gross Pathology, Examination, and Histological Analysis. On the tenth day of the experiment, mice were anesthetized and necropsied. Colons and livers were removed for gross pathologic evaluation. Colon lengths from all groups were recorded.

The colons and livers were weighed (50−100 mg) and homogenized with ice-cold PBS using a Tissuelyser-FEII system (Jingxin, China). In addition, the total protein concentration was measured via the BCA method. On the other hand, a portion of the colon and liver were immediately fixed in 4% buffered formalin. Fixed tissues were further transferred to an automatic tissue processor (Leica, Germany). Sections were stained with hematoxylin and eosin. All slides were photographed with a DM6B microscope (Leica, Germany) in a blinded manner.

Clinical Biochemistry Analyses. The levels of H_2O_2, MDA (A003-1-1, Nanjing Jiancheng), and the activities of CAT (A007-1-1, Nanjing Jiancheng) and SOD (A001-3-1, Nanjing Jiancheng) were determined according to the instructions of kits. A mouse IL-1β ELISA kit (Ml063132, Mlbio), mouse TNF-α ELISA kit (Ml002095, Mlbio), and mouse MPO ELISA kit (Ml002070, Mlbio) were used for cytokine measurement. Besides, the levels of alanine aminotransferase (C009-2-1, Nanjing Jiancheng) and aspartate aminotransferase (C010-2-1, Nanjing Jiancheng) in collected serum and liver homogenates were analyzed.

Gut Microbiota Analyses. Total DNA was extracted from the colonic contents using a QIAamp DNA Stool Mini Kit (51504, Qiagen). The V3−V4 regions of the 16S rRNA genes were amplified using the former primer: 341F (5′-CCTACGGGNGGCWGCAG-3′) and the reverse primer: 805R (5′-GACTACHVGGGTATCTAATCC-3′). Then, 16S rRNA genes were sequenced on an Illumina NovaSeq. 6000 platform (Illumina) to generate 2×250 paired-end reads.

High-quality reads were pooled for operational taxonomic unit (OTU) comparison and taxonomic abundance analysis. α and β diversity analyses were conducted using QIIME 2 software and R software (Version 4.0.5). For α diversity, the observed OTUs and Shannon diversity index were analyzed. For β diversity, NMDS was performed using unweighted UniFrac.

Statistical Analysis. Statistical analysis was performed using GraphPad Prism 7 (GraphPad Software). The results are presented as the mean ± standard error of the mean (S.E.M.). Student *t*-test was used to compare differences between the two groups. One-way ANOVA with Dunnett's test was used to compare differences between the three groups. Two-way ANOVA with Tukey's multiple-comparison tests was used to evaluate experiments involving multiple groups. Probability (P) values of <0.05 were considered significant. We estimated the variation within each experimental group and ensured that the variance was similar among groups that were statistically compared.

■ ASSOCIATED CONTENT

ⓢ Supporting Information

The Supporting Information is available free of charge at https://pubs.acs.org/doi/10.1021/acsami.1c09215.

The synthetic route of β-cyclodextrin (β-CD) conjugated with Tempol (TPL) units (TCD); characterization of

TCD by FT-IR and ¹H-NMR spectroscopy; design and observation of GEN-NPs; characterization of GEN-NPs; ROS-scavenging capability of different materials; cellular uptake and *in vitro* cytotoxicity studies of GEN-NPs; *in vitro* antioxidative stress activities and *in vitro* cytotoxicity studies of GEN-NPs; GEN-NPs regulate autophagy-inflammasome signaling pathway in NCM-460 cells; GEN-NPs preferentially localize to the inflamed colon; toxicity study of oral administration of GEN-NPs in mice; and analysis of the inflammation and gut microbiota in colitis mice after treatment with GEN-NPs (PDF)

■ AUTHOR INFORMATION

Corresponding Author

Suquan Song − *MOE Joint International Research Laboratory of Animal Health and Food Safety, College of Veterinary Medicine, Nanjing Agricultural University, Nanjing 210095, P. R. China;* ◉ orcid.org/0000-0002-1350-3825; Email: suquan.song@njau.edu.cn

Authors

Wentao Fan − *MOE Joint International Research Laboratory of Animal Health and Food Safety, College of Veterinary Medicine, Nanjing Agricultural University, Nanjing 210095, P. R. China*

Shuo Zhang − *MOE Joint International Research Laboratory of Animal Health and Food Safety, College of Veterinary Medicine, Nanjing Agricultural University, Nanjing 210095, P. R. China*

Yuting Wu − *MOE Joint International Research Laboratory of Animal Health and Food Safety, College of Veterinary Medicine, Nanjing Agricultural University, Nanjing 210095, P. R. China*

Tao Lu − *Joint Laboratory of Advanced Biomedical Materials (NFU-UGent), Jiangsu Co-Innovation Center of Efficient Processing and Utilization of Forest Resources, Nanjing Forestry University, Nanjing 210037, P. R. China*

Jiwen Liu − *MOE Joint International Research Laboratory of Animal Health and Food Safety, College of Veterinary Medicine, Nanjing Agricultural University, Nanjing 210095, P. R. China*

Xiuyun Cao − *MOE Joint International Research Laboratory of Animal Health and Food Safety, College of Veterinary Medicine, Nanjing Agricultural University, Nanjing 210095, P. R. China; Jiangsu Engineering Laboratory of Animal Immunology, Institute of Immunology and College of Veterinary Medicine, Nanjing Agricultural University, Nanjing 210095, P. R. China*

Shuhui Liu − *MOE Joint International Research Laboratory of Animal Health and Food Safety, College of Veterinary Medicine, Nanjing Agricultural University, Nanjing 210095, P. R. China*

Liping Yan − *MOE Joint International Research Laboratory of Animal Health and Food Safety, College of Veterinary Medicine, Nanjing Agricultural University, Nanjing 210095, P. R. China; Jiangsu Engineering Laboratory of Animal Immunology, Institute of Immunology and College of Veterinary Medicine, Nanjing Agricultural University, Nanjing 210095, P. R. China*

Xizhi Shi − *School of Marine Sciences, Ningbo University, Ningbo 315211, P. R. China*

Guangliang Liu − *State Key Laboratory of Veterinary Etiological Biology, Lanzhou Veterinary Research Institute, Chinese Academy of Agricultural Sciences, Lanzhou 730046, P. R. China;* ◉ orcid.org/0000-0001-8158-5749

Chaobo Huang − *Joint Laboratory of Advanced Biomedical Materials (NFU-UGent), Jiangsu Co-Innovation Center of Efficient Processing and Utilization of Forest Resources, Nanjing Forestry University, Nanjing 210037, P. R. China;* ◉ orcid.org/0000-0003-3484-0545

Complete contact information is available at:
https://pubs.acs.org/10.1021/acsami.1c09215

Author Contributions

S.S. conceived the project; W.F. and S.S. wrote the paper; W.F. performed most of the experiments; W.F. and S.Z. analyzed the data; S.Z., Y.W., T.L., J.L., X.C., and S.L. contributed to some of the experiments. L.Y., X.S., G.L., and C.H. revised the paper. All authors have approved the final version of the manuscript.

Notes

The authors declare no competing financial interest.

■ ACKNOWLEDGMENTS

■ ABBREVIATIONS

IBD, inflammatory bowel disease
GEN, genistein
ROS, reactive oxygen species
NPs, nanoparticles
ERβ, estrogen receptor β
ASC, apoptosis-associated speck-like protein containing a CARD
LPS, lipopolysaccharide
DSS, dextran sulfate sodium salt
IL-1β, interlukin-1β
TNF-α, tumor necrosis factor α
CD, Crohn's disease
UC, ulcerative colitis
CDI, 1,1-carbonyldiimidazole
DMAP, 4-dimethylaminopyridine
DCM, dichloromethane
THF, tetrahydrofuran
DIC, N,N'-diisopropylcarbodiimide
TPL, tempol
β-CD, β-cyclodextrin
TCD, TPL-conjugated β-CD
SOD, superoxide dismutase
HMPBA-Pin, 4-(hydroxymethyl)phenylboronic acid pinacol ester
TPGS, D-α-tocopherol poly(ethylene glycol) 1000 succinate
NMR, nuclear magnetic resonance
FT-IR, Fourier transform infrared
ESI-MS, electrospray ionization mass spectrometry
UV, ultraviolet

SEM, scanning electron microscopy
TEM, transmission electron microscopy
DSC, differential scanning calorimetry
H_2O_2, hydrogen peroxide
CAT, catalase
$O_2^{\bullet-}$, superoxide anion
DPPH, 2,2-diphenyl-1-picrylhydrazyl
DAPI, 4′,6-diamidino-2-phenylindole
DCF-DA, 2′,7′-dichlorofluorescein-diacetate
ELISA, enzyme-linked immunosorbent assay
ATG16L1, autophagy-related 16 like 1
ULK1, unc-51 like autophagy activating kinase 1
LC3B, light chain 3B
SGF, simulated gastric fluids
SIF, simulated intestinal fluids
SCF, simulated colonic fluids
HPLC, high-performance liquid chromatography
GC, gastric contents
CC, colonic contents
DAI, disease activity index
MDA, malondialdehyde
MPO, myeloperoxidase
NMDS, nonmetric multidimensional scaling
DMEM, Dulbecco's modified Eagle's medium
CCK-8, cell counting kit-8
S.E.M., standard error of the mean

■ REFERENCES

(1) Cainzos-Achirica, M.; Glassner, K.; Zawahir, H. S.; Dey, A. K.; Agrawal, T.; Quigley, E. M. M.; Abraham, B. P.; Acquah, I.; Yahya, T.; Mehta, N. N.; Nasir, K. Inflammatory Bowel Disease and Athero-sclerotic Cardiovascular Disease: JACC Review Topic of the Week. *J. Am. Coll. Cardiol.* **2020**, *76*, 2895−2905.

(2) Kaplan, G. G.; Windsor, J. W. The Four Epidemiological Stages in the Global Evolution of Inflammatory Bowel Disease. *Nat. Rev. Gastroenterol. Hepatol.* **2021**, *18*, 56−66.

(3) Irvine, E. J.; Marshall, J. K. Increased Intestinal Permeability Precedes the Onset of Crohn's Disease in A Subject with Familial Risk. *Gastroenterology* **2000**, *119*, 1740−1744.

(4) Xavier, R. J.; Podolsky, D. K. Unravelling the Pathogenesis of Inflammatory Bowel Disease. *Nature* **2007**, *448*, 427−434.

(5) Chang, J. T. Pathophysiology of Inflammatory Bowel Diseases. *N. Engl. J. Med.* **2020**, *383*, 2652−2664.

(6) Neurath, M. F.; Finotto, S. The Many Roads to Inflammatory Bowel Diseases. *Immunity* **2006**, *25*, 189−191.

(7) Bhattacharyya, A.; Chattopadhyay, R.; Mitra, S.; Crowe, S. E. Oxidative Stress: an Essential Factor in the Pathogenesis of Gastro-intestinal Mucosal Diseases. *Physiol. Rev.* **2014**, *94*, 329−354.

(8) Yang, X.; Mao, Z.; Huang, Y.; Yan, H.; Yan, Q.; Hong, J.; Fan, J.; Yao, J. Reductively Modified Albumin Attenuates DSS-Induced Mouse Colitis through Rebalancing Systemic Redox State. *Redox Biol.* **2021**, *41*, No. 101881.

(9) Yin, Y.; Yang, J.; Pan, Y.; Gao, Y.; Huang, L.; Luan, X.; Lin, Z.; Zhu, W.; Li, Y.; Song, Y. Mesopore to Macropore Transformation of Metal-Organic Framework for Drug Delivery in Inflammatory Bowel Disease. *Adv. Healthcare Mater.* **2021**, *10*, No. 2000973.

(10) Du, Y.; Rong, L.; Cong, Y.; Shen, L.; Zhang, N.; Wang, B. Macrophage Polarization: An Effective Approach to Targeted Therapy of Inflammatory Bowel Disease. *Expert Opin. Ther. Targets* **2021**, *25*, 191−209.

(11) Khare, T.; Palakurthi, S. S.; Shah, B. M.; Palakurthi, S.; Khare, S. Natural Product-Based Nanomedicine in Treatment of Inflammatory Bowel Disease. *Int. J. Mol. Sci.* **2020**, *21*, No. 3956.

(12) Debnath, T.; Kim, D. H.; Lim, B. O. Natural Products as A Source of Anti-Inflammatory Agents Associated with Inflammatory Bowel Disease. *Molecules* **2013**, *18*, 7253−7270.

(13) Mukund, V.; Mukund, D.; Sharma, V.; Mannarapu, M.; Alam, A. Genistein: Its Role in Metabolic Diseases and Cancer. *Crit. Rev. Oncol. Hematol.* **2017**, *119*, 13−22.

(14) Rahman Mazumder, M. A.; Hongsprabhas, P. Genistein as Antioxidant and Antibrowning Agents in in vivo and in vitro: A Review. *Biomed. Pharmacother.* **2016**, *82*, 379−392.

(15) Tanideh, N.; Sadeghi, F.; Amanat, S.; Firoozi, D.; Noorafshan, A.; Iraji, A.; Koohi-Hosseinabadi, O. Protection by Pure and Genistein Fortified Extra Virgin Olive Oil, Canola Oil, and Rice Bran Oil against Acetic Acid-Induced Ulcerative Colitis in Rats. *Food Funct.* **2020**, *11*, 860−870.

(16) Chen, Y.; Le, T. H.; Du, Q.; Zhao, Z.; Liu, Y.; Zou, J.; Hua, W.; Liu, C.; Zhu, Y. Genistein Protects Against DSS-Induced Colitis by Inhibiting NLRP3 Inflammasome via TGR5-cAMP Signaling. *Int. Immunopharmacol.* **2019**, *71*, 144−154.

(17) Vanden Braber, N. L.; Novotny Nuñez, I.; Bohl, L.; Porporatto, C.; Nazar, F. N.; Montenegro, M. A.; Correa, S. G. Soy Genistein Administered in Soluble Chitosan Microcapsules Maintains Antioxidant Activity and Limits Intestinal Inflammation. *J. Nutr. Biochem.* **2018**, *62*, 50−58.

(18) Abron, J. D.; Singh, N. P.; Price, R. L.; Nagarkatti, M.; Nagarkatti, P. S.; Singh, U. P. Genistein Induces Macrophage Polarization and Systemic Cytokine to Ameliorate Experimental Colitis. *PLoS One* **2018**, *13*, No. e0199631.

(19) Xiao, Y.; Ho, C.-T.; Chen, Y.; Wang, Y.; Wei, Z.; Dong, M.; Huang, Q. Synthesis, Characterization, and Evaluation of Genistein-Loaded Zein/Carboxymethyl Chitosan Nanoparticles with Improved Water Dispersibility, Enhanced Antioxidant Activity, and Controlled Release Property. *Foods* **2020**, *9*, No. 1604.

(20) Luo, X. M.; Yan, C.; Feng, Y. M. Nanomedicine for the Treatment of Diabetes-Associated Cardiovascular Diseases and Fibrosis. *Adv. Drug Delivery Rev.* **2021**, *172*, 234−248.

(21) Liu, Y.; Li, D.; Ding, J.; Chen, X. Controlled synthesis of polypeptides. *Chin. Chem. Lett.* **2020**, *31*, 3001−3014.

(22) Wei, L.; Chen, J.; Ding, J. Sequentially stimuli-responsive anticancer nanomedicines. *Nanomedicine* **2021**, *16*, 261−264.

(23) Chung, C. H.; Jung, W.; Keum, H.; Kim, T. W.; Jon, S. Nanoparticles Derived from the Natural Antioxidant Rosmarinic Acid Ameliorate Acute Inflammatory Bowel Disease. *ACS Nano* **2020**, *14*, 6887−6896.

(24) Sohail, M.; Mudassir; Minhas, M. U.; Khan, S.; Hussain, Z.; de Matas, M.; Shah, S. A.; Khan, S.; Kousar, M.; Ullah, K. Natural and Synthetic Polymer-Based Smart Biomaterials for Management of Ulcerative Colitis: a Review of Recent Developments and Future Prospects. *Drug Delivery Transl. Res.* **2019**, *9*, 595−614.

(25) Nakkala, J. R.; Li, Z.; Ahmad, W.; Wang, K.; Gao, C. Immunomodulatory Biomaterials and Their Application in Therapies for Chronic Inflammation-Related Diseases. *Acta Biomater.* **2021**, *123*, 1−30.

(26) Wilson, D. S.; Dalmasso, G.; Wang, L.; Sitaraman, S. V.; Merlin, D.; Murthy, N. Orally delivered thioketal nanoparticles loaded with TNF-α−siRNA target inflammation and inhibit gene expression in the intestines. *Nat. Mater.* **2010**, *9*, 923−928.

(27) Zhang, Q.; Tao, H.; Lin, Y.; Hu, Y.; An, H.; Zhang, D.; Feng, S.; Hu, H.; Wang, R.; Li, X.; Zhang, J. A superoxide dismutase/catalase mimetic nanomedicine for targeted therapy of inflammatory bowel disease. *Biomaterials* **2016**, *105*, 206−221.

(28) Dev, A.; Sardoiwala, M. N.; Kushwaha, A. C.; Karmakar, S.; Choudhury, S. R. Genistein Nanoformulation Promotes Selective Apoptosis in Oral Squamous Cell Carcinoma through Repression of 3PK-EZH2 Signalling Pathway. *Phytomedicine* **2021**, *80*, No. 153386.

(29) Botet-Carreras, A.; Tamames-Tabar, C.; Salles, F.; Rojas, S.; Imbuluzqueta, E.; Lana, H.; Blanco-Prieto, M. J.; Horcajada, P. Improving the Genistein Oral Bioavailability via Its Formulation into the Metal−Organic Framework MIL-100(Fe). *J. Mater. Chem. B* **2021**, *9*, 2233−2239.

(30) Zhang, Q.; Zhang, F.; Chen, Y.; Dou, Y.; Tao, H.; Zhang, D.; Wang, R.; Li, X.; Zhang, J. Structure−Property Correlations of Reactive Oxygen Species-Responsive and Hydrogen Peroxide-Eliminating

Materials with Anti-Oxidant and Anti-Inflammatory Activities. *Chem. Mater.* **2017**, *29*, 8221−8238.

(31) Lewis, P. T.; Wähälä, K.; Hoikkala, A.; Mutikainen, I.; Meng, Q.-H.; Adlercreutz, H.; Tikkanen, M. J. Synthesis of Antioxidant Isoflavone Fatty Acid Esters1. *Tetrahedron* **2000**, *56*, 7805−7810.

(32) Zuo, R.; Zhang, J.; Song, X.; Hu, S.; Gao, X.; Wang, J.; Ji, H.; Ji, C.; Peng, L.; Si, H.; Li, G.; Fang, K.; Zhang, J.; Jiang, S.; Guo, D. Encapsulating Halofuginone Hydrobromide in TPGS Polymeric Micelles Enhances Efficacy Against Triple-Negative Breast Cancer Cells. *Int. J. Nanomed.* **2021**, *16*, 1587−1600.

(33) Mittal, P.; Vrdhan, H.; Ajmal, G.; Bonde, G.; Kapoor, R.; Mishra, B. Formulation and Characterization of Genistein-loaded Nano-structured Lipid Carriers: Pharmacokinetic, Biodistribution and In vitro Cytotoxicity Studies. *Curr. Drug Delivery* **2019**, *16*, 215−225.

(34) Lv, S.; Wu, Y.; Cai, K.; He, H.; Li, Y.; Lan, M.; Chen, X.; Cheng, J.; Yin, L. High Drug Loading and Sub-Quantitative Loading Efficiency of Polymeric Micelles Driven by Donor-Receptor Coordination Interactions. *J. Am. Chem. Soc.* **2018**, *140*, 1235−1238.

(35) Wang, Y.; Li, L.; Zhao, W.; Dou, Y.; An, H.; Tao, H.; Xu, X.; Jia, Y.; Lu, S.; Zhang, J.; Hu, H. Targeted Therapy of Atherosclerosis by a Broad-Spectrum Reactive Oxygen Species Scavenging Nanoparticle with Intrinsic Anti-inflammatory Activity. *ACS Nano* **2018**, *12*, 8943−8960.

(36) Hui, Y.; Wen, S.; Lihong, W.; Chuang, W.; Chaoyun, W. Molecular Structures of Nonvolatile Components in the Haihong Fruit Wine and Their Free Radical Scavenging Effect. *Food Chem.* **2021**, *353*, No. 129298.

(37) Mehandru, S.; Colombel, J.-F. The intestinal barrier, an arbitrator turned provocateur in IBD. *Nat. Rev. Gastroenterol. Hepatol.* **2021**, *18*, 83−84.

(38) Patankar, J. V.; Becker, C. Cell Death in the Gut Epithelium and Implications for Chronic Inflammation. *Nat. Rev. Gastroenterol. Hepatol.* **2020**, *17*, 543−556.

(39) Choo, P.; Liu, T.; Odom, T. W. Nanoparticle Shape Determines Dynamics of Targeting Nanoconstructs on Cell Membranes. *J. Am. Chem. Soc.* **2021**, *143*, 4550−4555.

(40) Ma, M.; Chen, Y.; Zhao, M.; Sui, J.; Guo, Z.; Yang, Y.; Xu, Z.; Sun, Y.; Fan, Y.; Zhang, X. Hierarchical Responsive Micelle Facilitates Intratumoral Penetration by Acid-Activated Positive Charge Surface and Size Contraction. *Biomaterials* **2021**, *271*, No. 120741.

(41) Bou-Teen, D.; Kaludercic, N.; Weissman, D.; Turan, B.; Maack, C.; Di Lisa, F.; Ruiz-Meana, M. Mitochondrial ROS and Mitochondria-Targeted Antioxidants in the Aged Heart. *Free Radical Biol. Med.* **2021**, *167*, 109−124.

(42) Zhang, K.; Kaufman, R. J. From Endoplasmic-Reticulum Stress to the Inflammatory Response. *Nature* **2008**, *454*, 455−462.

(43) Yang, B.; Chen, Y.; Shi, J. Reactive Oxygen Species (ROS)-Based Nanomedicine. *Chem. Rev.* **2019**, *119*, 4881−4985.

(44) Deets, K. A.; Vance, R. E. Inflammasomes and Adaptive Immune Responses. *Nat. Immunol.* **2021**, *22*, 412−422.

(45) Deretic, V. Autophagy in Inflammation, Infection, and Immunometabolism. *Immunity* **2021**, *54*, 437−453.

(46) Nielsen, A. J.; McNulty, J. Polyphenolic Natural Products and Natural Product-Inspired Steroidal Mimics as Aromatase Inhibitors. *Med. Res. Rev.* **2019**, *39*, 1274−1293.

(47) Mal, R.; Magner, A.; David, J.; Datta, J.; Vallabhaneni, M.; Kassem, M.; Manouchehri, J.; Willingham, N.; Stover, D.; Vandeusen, J.; Sardesai, S.; Williams, N.; Wesolowski, R.; Lustberg, M.; Ganju, R. K.; Ramaswamy, B.; Cherian, M. A. Estrogen Receptor Beta (ERβ): A Ligand Activated Tumor Suppressor. *Front. Oncol.* **2020**, *10*, No. 587386.

(48) Hases, L.; Indukuri, R.; Birgersson, M.; Nguyen-Vu, T.; Lozano, R.; Saxena, A.; Hartman, J.; Frasor, J.; Gustafsson, J.; Katajisto, P.; Archer, A.; Williams, C. Intestinal Estrogen Receptor Beta Suppresses Colon Inflammation and Tumorigenesis in Both Sexes. *Cancer Lett.* **2020**, *492*, 54−62.

(49) Tao, Y.; Yue, M.; Lv, C.; Yun, X.; Qiao, S.; Fang, Y.; Wei, Z.; Xia, Y.; Dai, Y. Pharmacological Activation of ERβ by Arctigenin Maintains

the Integrity of Intestinal Epithelial Barrier in Inflammatory Bowel Diseases. *FASEB J.* **2020**, *34*, 3069−3090.

(50) Song, P.; Li, Y.; Dong, Y.; Liang, Y.; Qu, H.; Qi, D.; Lu, Y.; Jin, X.; Guo, Y.; Jia, Y.; Wang, X.; Xu, W.; Quan, C. Estrogen Receptor β Inhibits Breast Cancer Cells Migration and Invasion through CLDN6-Mediated Autophagy. *J. Exp. Clin. Cancer Res.* **2019**, *38*, No. 354.

(51) Wei, Y.; Zhou, J.; Wu, J.; Huang, J. ERβ Promotes Aβ Degradation via the Modulation of Autophagy. *Cell Death Dis.* **2019**, *10*, No. 565.

(52) Wei, Y.; Huang, C.; Wu, H.; Huang, J. Estrogen Receptor Beta (ERβ) Mediated-CyclinD1 Degradation via Autophagy Plays an Anti-Proliferation Role in Colon Cells. *Int. J. Biol. Sci.* **2019**, *15*, 942−952.

(53) Li, C. W.; Zhao, Y.; Cheng, J.; Guo, J. W.; Zhang, Q. X.; Zhang, X. J.; Ren, J.; Wang, F. C.; Huang, J.; Hu, H. Y.; Wang, R. B.; Zhang, J. X. A Proresolving Peptide Nanotherapy for Site-Specific Treatment of Inflammatory Bowel Disease by Regulating Proinflammatory Micro-environment and Gut Microbiota. *Adv. Sci.* **2019**, *6*, No. 1900610.

(54) Parker, B. J.; Wearsch, P. A.; Veloo, A. C. M.; Rodriguez-Palacios, A. The Genus Alistipes: Gut Bacteria With Emerging Implications to Inflammation, Cancer, and Mental Health. *Front. Immunol.* **2020**, *11*, No. 906.

(55) Wu, M.; Li, P.; An, Y.; Ren, J.; Yan, D.; Cui, J.; Li, D.; Li, M.; Wang, M.; Zhong, G. Phloretin Ameliorates Dextran Sulfate Sodium-Induced Ulcerative Colitis in Mice by Regulating the Gut Microbiota. *Pharmacol. Res.* **2019**, *150*, No. 104489.

(56) Guo, S.; Geng, W.; Chen, S.; Wang, L.; Rong, X.; Wang, S.; Wang, T.; Xiong, L.; Huang, J.; Pang, X.; Lu, Y. Ginger Alleviates DSS-Induced Ulcerative Colitis Severity by Improving the Diversity and Function of Gut Microbiota. *Front. Pharmacol.* **2021**, *12*, No. 632569.

(57) Xiao, J.; Chen, H.; Kang, D.; Shao, Y.; Shen, B.; Li, X.; Yin, X.; Zhu, Z.; Li, H.; Rao, T.; Xie, L.; Wang, G.; Liang, Y. Qualitatively and Quantitatively Investigating the Regulation of Intestinal Microbiota on the Metabolism of Panax Notoginseng Saponins. *J. Ethnopharmacol.* **2016**, *194*, 324−336.

(58) Yoon, H. S.; Cho, C. H.; Yun, M. S.; Jang, S. J.; You, H. J.; Kim, J. H.; Han, D.; Cha, K. H.; Moon, S. H.; Lee, K.; Kim, Y. J.; Lee, S. J.; Nam, T. W.; Ko, G. Akkermansia Muciniphila Secretes a Glucagon-Like Peptide-1-Inducing Protein that Improves Glucose Homeostasis and Ameliorates Metabolic Disease in Mice. *Nat. Microbiol.* **2021**, *6*, 563−573.

(59) Mithul Aravind, S.; Wichienchot, S.; Tsao, R.; Ramakrishnan, S.; Chakkaravarthi, S. Role of Dietary Polyphenols on Gut Microbiota, Their Metabolites and Health Benefits. *Food Res. Int.* **2021**, *142*, No. 110189.

(60) Andrade, F. O.; Liu, F.; Zhang, X.; Rosim, M. P.; Dani, C.; Cruz, I.; Wang, T. T. Y.; Helferich, W.; Li, R. W.; Hilakivi-Clarke, L. Genistein Reduces the Risk of Local Mammary Cancer Recurrence and Ameliorates Alterations in the Gut Microbiota in the Offspring of Obese Dams. *Nutrients* **2021**, *13*, No. 201.

(61) Ortega-Santos, C. P.; Al-Nakkash, L.; Whisner, C. M. Exercise and/or Genistein Treatment Impact Gut Microbiota and Inflammation after 12 Weeks on a High-Fat, High-Sugar Diet in C57BL/6 Mice. *Nutrients* **2020**, *12*, No. 3410.

(62) Yang, R.; Jia, Q.; Mehmood, S.; Ma, S.; Liu, X. Genistein Ameliorates Inflammation and Insulin Resistance through Mediation of Gut Microbiota Composition in Type 2 Diabetic Mice. *Eur. J. Nutr.* **2021**, *60*, 2155−2168.

(63) Li, L.; Guo, J.; Wang, Y.; Xiong, X.; Tao, H.; Li, J.; Jia, Y.; Hu, H.; Zhang, J. A Broad-Spectrum ROS-Eliminating Material for Prevention of Inflammation and Drug-Induced Organ Toxicity. *Adv. Sci.* **2018**, *5*, No. 1800781.

(64) Zhang, G.; Liao, Q.; Liu, Y.; Wang, L.; Gou, H.; Ke, C.; Huang, X.; Xi, K.; Jia, X. Secondary Structure-Induced Aggregation by Hydrogen Peroxide: a Stimuli-Triggered Open/Close Implementation by Recombination. *Nanoscale* **2018**, *10*, 5503−5514.